

Multi-year Evaluation of Airborne Geodetic Surveys to Estimate Seasonal Mass Balance, Columbia and Rocky Mountains, Canada

Ben M. Pelto¹, Brian Menounos¹, Shawn J. Marshall²

¹Natural Resources and Environmental Studies Institute and Geography Program, University of Northern British Columbia,
5 Prince George, V2N 4Z9, Canada

²Department of Geography, University of Calgary, Calgary, T2N 1N4, Canada

Correspondence to: Ben M. Pelto (pelto@unbc.ca)

Abstract. Seasonal measurements of glacier mass balance provide insight into the relation between climate forcing and glacier change. To evaluate the feasibility of using remotely sensed methods to assess seasonal balance we completed tandem airborne 10 laser scanning surveys (ALS) and field-based glaciological measurements over a four-year period for six alpine glaciers that lie in  Columbia and Rocky Mountains, near the headwaters of the Columbia River, British Columbia, Canada. We calculated annual geodetic balance using coregistered late summer digital elevation models (DEMs), and distributed estimates of density based on surface classification of ice, snow and firn surfaces. Winter balance was derived using coregistered late summer and spring DEMs, and density measurements from regional snow survey observations and our glaciological measurements. 15 Geodetic summer balance was calculated as the difference between winter and annual balance. Winter mass balance from our glaciological observations averaged 1.95 ± 0.09 m w.e., 4% greater than those derived from geodetic surveys. Average glaciological summer and annual balance were 3% smaller and 3% larger respectively, than our geodetic estimates. We find that distributing snow, firn and ice density based on surface classification has a greater influence on geodetic annual mass change than the density values themselves. Our results demonstrate that accurate assessments of seasonal mass change can be 20 produced using ALS over a series of glaciers spanning several mountain ranges. Such agreement over multiple seasons, years, and glaciers demonstrates the ability of high-resolution geodetic methods to increase the number of glaciers where seasonal mass balance can be reliably measured 

1 Introduction

Glaciers are in rapid retreat across western Canada (Menounos et al., 2018). Deglaciation is projected to have pronounced 25 impacts on streamflow in western Canada (Clarke et al., 2015), with greatest reductions in August and September streamflow as glaciers shrink (Huss and Hock, 2018; Jost et al., 2012). In the Canadian Columbia River Basin, peak glacier runoff from ice wastage is either currently underway (Huss and Hock, 2018) or will occur within the next decade (Clarke et al., 2015). Improved projections of changes in glacier runoff will require refined treatment of seasonally-varying processes that nourish and deplete glaciers, namely the re-distribution of snow by wind and gravitational processes and changes in surface albedo.

30 Seasonal mass balance records are also required to calibrate and validate these physically-based mass balance models. These records do not currently exist for the Columbia River Basin, however.

In addition to their use in refining estimates of future changes in glacier runoff, mass balance observations provide a valuable synopsis of a glacier's mass budget and its implications for glacier runoff (Jost et al., 2012; Ragettli et al., 2016; Stahl and Moore, 2006), water storage, regional climate (Huss et al., 2008; Radić and Hock, 2014), and contribution to sea level rise
35 (Huss and Hock, 2018). Glacier mass balance is a function of accumulation and ablation processes, responding directly to meteorological forcing at timescales of a season or more (Oerlemans et al., 1998). Measurement of seasonal mass change via in situ and geodetic methods provides a means to assess the importance of meteorological drivers of glacier nourishment and melt. These observations can reveal trends and patterns in glacier mass evolution, and are valuable calibration and validation datasets for global (Huss and Hock, 2018; Maussion et al., 2019) and regional glacier models (Clarke et al., 2015), and for
40 ingestion into regional hydrologic models (Schnorbus et al., 2014).

Seasonal balance is logically and financially difficult and globally, few seasonal mass balance records exist (Ohmura, 2011). Currently, seasonal balance measurements for western Canadian glaciers are not publicly available (WGMS, 2018). Seasonal snowpack forms a critical component of glacier mass balance (Østrem and Brugman, 1991); it controls the volume and timing of runoff in the snowmelt-dominated tributaries to the Columbia River (Brahney et al., 2017). Like many regions (Barnett et
45 al., 2005), high elevation snow and precipitation records are limited in the Columbia River Basin of Canada. Snow data are routinely only monitored at or below treeline, and much of the basin, including its glaciated terrain, exists above this elevation. Some models suggest snowpack may be increasing at high elevations (Schnorbus et al., 2014), though existing snow observations below treeline indicate decreased water equivalent through the 1980–2011 period (Brahney et al., 2017). This data gap hinders accurate estimates of alpine snowpack in the region, critical for glacier nourishment, ecosystems, hydropower,
50 and flood forecasts (Hamlet et al., 2005).

Geodetic methods are now regularly used to measure seasonal snow depth on glaciers via surface (Helffricht et al., 2014; McGrath et al., 2015) or helicopter-borne ground penetrating radar (Dadic et al., 2010; Machguth et al., 2006; Sold et al., 2014), airborne laser scanning surveys-ALS (Helffricht et al., 2012, 2014; Sold et al., 2013), airborne photogrammetry (Nolan et al., 2015), and stereoscopic satellite imagery (Belart et al., 2017). C
55 eu^{et}etic surveys offer the ability to greatly expand the number of glaciers over which snow depth and mass change measurements can occur (Berthier et al., 2014; Nolan et al., 2015). For hydrological applications, snow depth must be converted into snow water equivalent (SWE), and thus snow density must be known or estimated. Physical modeling of snow density is difficult (Sold et al., 2014), and in situ density measurements are sparse, and are expensive in terms of cost and effort. Often density measurements show little relation to either elevation or
snow depth (Fausto et al., 2018; Machguth et al., 2006; McGrath et al., 2015), increasing the importance of in situ
60 measurements. Density thus introduces uncertainty to geodetic winter SWE estimates which are vital to calibrate and validate hydrological modeling, and to measure seasonal mass balance (Belart et al., 2017; Sold et al., 2013). The primary objective of our study is to evaluate the reliability of geodetic surveys and density assumptions for estimation of seasonal mass change of temperate glaciers over multiple years.

1.1 Study Area

65 1.1.1 Columbia Mountains

The transboundary Columbia River Basin (668,000 km²) spans seven U.S. states and British Columbia (BC), Canada. The Canadian portion of the Basin represents 15% of the watershed's total area, yet provides between 30–40% of its total runoff, largely due to the presence of mountainous terrain with high amounts of orographic precipitation and extensive glacial cover (Cohen et al., 2000; Hamlet and Lettenmaier, 1999). There are 2,200 glaciers covering 1,760 km² in the Columbia Mountains 70 (Bolch et al., 2010); these glaciers primarily exist within the Cariboo, Monashee, Selkirk, and Purcell ranges, with the highest elevations rising to over 3,000 m above sea level (asl).

The Columbia Mountains are transitional between maritime and continental (Demarchi, 2011). Monthly average temperatures in the Canadian Columbia River Basin (elevation range from 420 to 3700 m asl) range from -9.2°C in January to 13.3°C in July (Najafi et al., 2017; Schnorbus et al., 2014). General circulation is dominated by westerly flow, which brings consistent 75 Pacific moisture, particularly in the winter months. Approximately 65% of annual precipitation falls as snow, with snowfall possible throughout the year (Schnorbus et al., 2014). The snow accumulation season in both the Columbia and Canadian Rocky Mountains extends from October to May. The summer melt season runs from May through September. From 1981–2010, Rodgers Pass, located in the center of the Columbia Mountains (Figure 1), at an elevation of 1330 m asl, had an average annual temperature of +1.9°C, and an average winter (December–February) temperature of -8.0°C, and experienced 1056 ± 49 80 mm w.e. of precipitation through the accumulation season (October–April) (Environment Canada, 2019).

1.1.2 Rocky Mountains

The southern Canadian Rockies are located east from the Columbia Mountains (Figure 1) across the Rocky Mountain Trench and are home to 1090 glaciers covering 1350 km² (Bolch et al., 2010).

The eastern slopes of the Canadian Rocky Mountains experience a continental climate with mild summers and cold winters. 85 However, winter precipitation along the continental divide is greatly influenced by moist Pacific air masses, with persistent westerly flow driving orographic uplift on the western flanks of the Rocky Mountains (Sinclair and Marshall, 2009). This combination of continental and maritime influences fosters extensive glaciation along the continental divide in the Canadian Rockies, with glaciers at elevations from 2200 to 3500 m asl on the eastern slopes. From 1981–2010, Lake Louise, located in 90 the center of the southern Canadian Rockies (Figure 1), at an elevation of 1524 m asl, had an average annual temperature of +0.2°C, an average winter temperature of -11.6°C, and experienced 298 ± 9 mm w.e. of precipitation through the accumulation season (Environment Canada, 2019). As evidenced by comparing Lake Louise and Rodgers Pass, the Canadian Rockies are drier and colder in winter than the Columbia Mountains.

2 Data and Methods

95 2.1 Study Sites

Over the period 2014–2018 we measured seasonal mass balance of six alpine glaciers (Table 1): (1) Zillmer Glacier (5.4 km^2) in the Cariboo Mountains, (2) Nordic Glacier (3.4 km^2) and (3) Illecillewaet Glacier (7.7 km^2) in the Selkirk Mountains, (4) Conrad Glacier (11.5 km^2) and (5) Kokanee Glacier (1.8 km^2) in the Purcell Mountains, and (6) Haig Glacier (2.6 km^2), which straddles the continental divide. Haig Glacier is in the Rocky Mountains, whereas the other five glaciers lie in the Columbia
100 Mountains.

2.2 Geodetic Mass Balance

We performed repeat fixed-wing ALS surveys from late summer 2014 to late summer 2016 (Table 2) using a Riegl VQ-580 infrared (1024 micron) laser scanner with dedicated Applanix POS AV Global Navigation Satellite System (GNSS) Inertial Measurement Unit (IMU). Later surveys used the same GNSS IMU and a Riegl VQ-780 infrared (1024 micron) laser scanner.
105 The VQ-580 and Q-780 were respectively flown at flying heights of around 500 and 2500 m above the terrain that yielded swath widths of 500-1000 m and 2000-3000 m. We planned the airborne surveys with 53% overlap between flight lines, to yield return point densities that averaged 1-3 laser shots m^{-2} (Table 2) with an effective sampling diameter of 10–20 cm per laser shot, and to minimize systematic bias from off-nadir laser shots.

2.2.1 ALS Post-Processing

110 Post-processing of the ALS survey flight trajectory data used the PosPac Mobile Mapping Suite (Applanix), with Trimble CenterPoint RTX with vertical and horizontal positional uncertainties that were typically better than $\pm 15 \text{ cm}$ (1σ). We post-processed point clouds and exported finished LAS files into LAStools (<https://rapidlasso.com/lastools/>) from which we used las2DEM to create 1 m resolution DEMs. Las2dem triangulates ground classified ALS points from las/laz files into a temporary triangulated irregular network (TIN). A DEM is then created from this using nearest neighbor interpolation. Given an average
115 point density of greater than 2 points m^{-2} (Table 2), little interpolation was required. We coregistered all DEMs following the method detailed in Nuth and Kääb (2011). For late summer surveys, one master DEM was chosen and all other late summer DEMs were coregistered to that DEM for stable surfaces only. Stable surfaces were identified in satellite imagery and excluded
forests, lakes and ice- and snow-covered areas. For winter DEMs, the previous late summer DEM was used as the master DEM
120 to mitigate against any surface height changes in areas defined as stable terrain, due to processes such as rockfall or vegetation height change. During the spring surveys, there was little to no snow-free terrain, except rocky features with extreme slopes which are not used in the coregistration (slope $>40^\circ$ excluded). We thus did not apply any vertical shift during coregistration of winter DEMs.

We utilized satellite imagery from Landsat 7 and 8, Sentinel-2, and Planet Scope at 30, 10, and 3–5 m resolution respectively (Bevington et al., 2018), to guide surface classification used to coregister DEMs and calculate geodetic mass change. We

125 selected the latest snow-free imagery from September or late August, and used a band ratio and threshold method (Kääb, 2005) to classify areas of snow, firn, and ice. In some cases, we manually corrected surface maps where our automated methods failed to differentiate between firn and snow surfaces.

To calculate annual mass change (B_a), we (1) difference two DEMs to create a height change DEM (ΔDEM), (2) bias correct the height change by the mean height difference over stable terrain between two DEMs after coregistration ($\text{Bias}_{\Delta h}$, Table 3), 130 (3) derive a mask based on surface classification of ice, firn and snow from satellite imagery (Figure S1), then (4) apply the density of each respective surface type (Table 4), to the ΔDEM to calculate mass balance. We chose not to use Digital Terrain Models (DTMs), which represent gridded elevation based on last returns from the laser scanner, since our gridding algorithms employed in LAStools filled crevasses and did not preserve sharp ridges that aided in coregistration of the DEMs.

Annual glacier mass balance is defined as the sum of accumulation and ablation throughout the balance year (Cuffey and 135 Paterson, 2010), which can be expressed as the sum of winter and summer balance:

$$B_a = B_w + B_s \quad (1)$$

For geodetic and glaciological mass balance, we measure winter and annual balance, and calculate summer balance as the difference between them:

$$B_s = B_a - B_w \quad (2)$$

140 To calculate geodetic winter balance ($B_{w\text{-geod}}$), we created a ΔDEM from a given spring DEM and the previous late summer DEM, then applied spring snow density (Table 4). We did not independently estimate $B_{s\text{-geod}}$ because of the added uncertainty of partitioning elevation change due to melt or compaction of snow/firn surfaces.

2.2.2 Density Estimates

While ALS provides an accurate estimate of snow depth with vertical uncertainties of $\pm 0.1\text{--}0.3$ m (Abermann et al., 2010; 145 Bollmann et al., 2011; Joerg et al., 2012), it provides no information regarding snow density. We use manual snow survey measurements available from the British Columbia River Forecast Center (BCRFC) (Weber and Litke, 2018) as independent data to estimate spring snow density, and compare this with our measured glaciological snow densities. These snow surveys are conducted as part of the BC snow survey program eight times per year, with most sites located between 1000 and 2000 m asl. We use these BCRFC data to evaluate whether reliable estimates of snow density can be obtained for regions where no 150 snow observations over glaciers exist. The mean date of our spring field visits was May 1st (Table 2), so we chose May 1st snow survey data ($n = 10,169$) to derive a relation between SWE (kg m^{-2}) and snow depth (m) (Figure 2). The linear relation (regression fit) yields a slope of $470 \pm 70 \text{ kg m}^{-3}$ ($r^2 = 0.97$), which we use as the average May 1st snow density which we applied for our geodetic B_w calculations. For Haig Glacier, we chose only snow survey measurements from the Rocky Mountains for a linear relation yielding $440 \pm 50 \text{ kg m}^{-3}$ ($n = 629$). The estimated uncertainty in bulk snow density (± 70 and 155 $\pm 50 \text{ kg m}^{-3}$) represents the standard deviation (σ) of the snow survey data. For our glaciological density-informed $B_{w\text{-geod}}$, we use the observed glacier-wide snow density (Table S1) and a linear regression of density versus day and used the slope ($3.0 \text{ kg m}^{-3} \text{ day}^{-1}$, $r^2 = 0.43$) and days between the survey and the observations to adjust for change in snow density (Figure 3). The

lack of an altitudinal trend in snow density observed on many glaciers (Fausto et al., 2018; McGrath et al., 2015, 2018; Sold et al., 2016) and those of this study, coupled with the absence of high-elevation snow density measurements and the annual variability of snow density evolution, required the use of a single value for spring snow density.

Regional observations of late summer snow density are consistent (Table 5); ranging from $530\text{--}630\text{ kg m}^{-3}$ for glaciers across the Pacific Northwest (Table 5). This is expected for temperate, mid-latitude glaciers, where snow densities range from the “critical density” of about 550 kg m^{-3} (Benson, 1962; Herron and Langway, 1980) to around 600 kg m^{-3} depending upon regional climatology. Since we independently evaluate glaciological versus geodetic estimates of mass change, we compare application of our late summer glaciological snow density measurements to calculate net balance with estimates based on the average of typical observations from four regional sources ($590 \pm 60\text{ kg m}^{-3}$; Table 5), to test the impact of uncertainties of up to 10% in this parameter. Firn density has not been reported for the study area, so we estimate $700 \pm 100\text{ kg m}^{-3}$ for multi-year firn based on observations in the Alps (Ambach et al., 1966). This is also consistent with our firn core measurements for firn two or more years old (Table S2; average density of $703 \pm 65\text{ kg m}^{-3}$, n=4). Measurements of one-year-old firn averaged $619 \pm 47\text{ kg m}^{-3}$ (n=8). Given the sustained mass loss of Pacific Northwest glaciers (Bolch et al., 2010; Menounos et al., 2018; Pelto, 2006), exposed firn is generally more than one year old, and we apply an uncertainty of two times the σ of our multi-year firn core observations ($\pm 15\%$), which captures the range of observed firn densities ($664\text{--}776\text{ kg m}^{-3}$). We use an ice density of $910 \pm 10\text{ kg m}^{-3}$ (Clarke et al., 2013). After performing a pixel-based surface classification for each late summer, we used these classification masks to assign a density (Table 4) to each pixel (snow/firn/ice).

2.2.3 Firn Processes

Firn meltwater retention and densification are neglected in our study. Firn densification (Belart et al., 2017; Sold et al., 2013) can be modeled, but this approach assumes that net annual surface elevation change corresponds to the average annual accumulation layer transformed from end-of-year snow density to ice (Sold et al., 2013). Glaciers in this study have a low average accumulation ablation area ratio (AAR, 0.38%, Table 3), and ice area ratios range from 0.38% to 0.94% (mean: 0.47%). In most years, a significant amount of multi-year firn is exposed on these glaciers, similar to other glaciers experiencing strong mass loss (Fischer, 2011; Klug et al., 2018). Firn area and thickness losses interrupt the normal cycle of firn densification. Using the firn model of Sold et al. (2013) yields an estimated annual surface lowering over a given accumulation area due to densification of $\sim 0.20\text{ m}$; yet uncertainty in estimating surface lowering resulting from densification is high since we lack knowledge of the required input parameters. Because of this, and because firn densification is unlikely to produce firn densities outside the range of our estimate ($700 \pm 100\text{ kg m}^{-3}$), we chose not to estimate firn densification in our study. Firn compaction therefore comprises one systematic uncertainty term in our analysis.

2.3 Glaciological Mass Balance

We collected glacier mass balance measurements using the glaciological method (Cogley et al., 2011) with a two season stratigraphic approach (Østrem and Brugman, 1991). Spring glaciological field campaigns typically occurred between mid-

190 April and mid-May, and the summer/annual balance visits took place between mid-August and mid-September (Table 2). Measurements of B_a and B_w allow the calculation of summer balance B_s (Eqn. 1). Glacier mass balance measurements included snow depth, snow density, ablation, and kinematic GPS surveys of the glacier surface (Figure 4).

195 Our methods apply to the four glaciers studied by UNBC: the Zillmer, Nordic, Conrad and Kokanee glaciers. For Haig Glacier, winter mass balance measurements followed the same field protocols, but summer mass balance is derived from a combination of point observations and a distributed model of glacier melt (Marshall, 2014; Samimi and Marshall, 2017). The glacier melt model has 30 m-resolution and uses a surface energy balance, driven by AWS data collected on the upper glacier and in the glacier forefield. Illecillewaet Glacier has been monitored by Parks Canada since 2009 (Hirose and Marshall, 2013). We calculated B_{a_glac} for Illecillewaet Glacier using the contour method since there were insufficient point measurements to estimate mass balance using the profile method.

200 Others have shown that snow depth is more variable than density (Elder et al., 1991; Pelto, 1996; Pulwicki et al., 2018), so we designed a sampling strategy that measures snow depth much more than density (an approximate sampling ratio of 25:1). We used G3 industrial aluminum probes to collect over 1,750 estimates of snow depth over the period of study. The probe can penetrate thick ice lenses and allowed us to measure snow depths of up to 8 m. The boundary between snow and firn is typically made up of clearly defined ice lenses of variable thickness, which can be detected with a probe on mid-latitude glaciers (Østrem and Brugman, 1991; Pelto, 1996; Sold et al., 2013). This end-of-summer surface at the glaciers in this study has such strength that an industrial probe can penetrate no more than a couple centimeters, in contrast with internal ice lenses in seasonal snowpack, which can be penetrated due to weak underlying support. Initially, we collected four probe measurements per location, but after two spring seasons we determined that two measurements were sufficient per location. The average σ for probe measurements for four (two) measurements was 0.14 m (0.07 m) for spring and 0.10 m (0.08 m) for late summer. Two 205 measurements per location allowed additional locations to be measured, since our observed low variability between proximal measurements is consistent with other studies (Beedle et al., 2014; Pelto et al., 2013).

210 We measured snow density with a 100 cm³ box cutter (Hydro-Tech) in snow pits and from snow cores using a 7.25 cm diameter Kovacs corer. Our rationale to use a snow corer was that average spring snow depth exceeded 4 m and we chose to have as many sites as possible to estimate snow density. The corer also allowed us to sample internal ice lenses, which are difficult to measure with a snow sampler (Proksch et al., 2016). We measured spring snow density at low, middle and high elevations for 215 each glacier. If we observed an elevation trend in our density measurements, we applied a linear regression of density and elevation to our depth measurements prior to converting these data to water equivalent (mass). When there was no linear gradient, we averaged the snow density measurements to produce a glacier-wide snow density.

220 We conducted nine side-by-side pit/core comparisons that revealed density measured in our snow pits was comparable, with density from snow pits about $0.2 \pm 5.7\%$ heavier than measured by subsampling snow cores (Figure S4). The mean absolute difference between pit and core density was 4.8%, similar to observations made at Alto dell'Ortles (Gabrielli et al., 2010). Methodological differences (S1) are within the range expected between duplicate field-based measurements of snow density (1-6%) and with different cutters (3-12%) (Conger and McClung, 2009; Proksch et al., 2016).

225 Aluminum and PVC ablation stakes were used on each glacier to measure ice and firn ablation. The stake heights were measured (± 1 cm) and redrilled during each late summer visit. As a check on stake elevation, we measured depth to the previous snow surface for all stakes in firn, as stakes may self-drill in firn (Østrem and Brugman, 1991). Stakes were generally aligned along the centerline of a given glacier; however, we added a second transect of stakes to cover each branch to improve spatial coverage on each study site (Figure 4). Conrad Glacier also featured three latitudinal sets of ablation stakes.

230 To calculate mass balance, we used the profile method (Escher-Vetter et al., 2009), applied over 100 m hypsometric elevation bins. The area-altitude distribution of a given glacier was obtained using our annual late summer ALS DEMs. The boundary of each glacier was manually delineated using the ALS DEM hillshade of the previous late summer, and a Δ DEM (Abermann et al., 2010). We also calculated mass balance using linear regression. For Zillmer, Nordic and Conrad glaciers, we separately considered the measurements from two distinct branches or sides of each glacier and then separately applied the profile and linear methods to each branch.

235 To account for mass change between a given field visit and the associated ALS survey, we completed kinematic GPS surveys using a Topcon GB-1000 receiver as a rover and a second receiver as a base station. We corrected base station data using Natural Resources Canada Precise Point Positioning (<https://webapp.geod.nrcan.gc.ca/geod/tools-outils/ppp.php>) before post-processed surveys using Topcon Tools. Height change observed between the ALS DEM surface and survey points were binned by elevation (Figure S5) and assigned a density based upon surface classification as determined from satellite imagery. Since 240 ALS surveys were essentially synchronous (typically flown over two to three days), we chose to apply the correction to the glaciological estimates of mass balance. We surveyed 2–6 control points at each site to determine the survey reliability and found that horizontal and vertical uncertainties respectively averaged ± 0.04 m and ± 0.06 m.

2.4 Uncertainty Assessment

245 We analyzed stable terrain to derive statistical indicators of bias and data dispersion from Δ DEM using a late summer DEM as a reference. We report the mean, median and normalized median absolute deviation (NMAD) over stable terrain (Table 3), which generally covered 10–20 km². To calculate uncertainty in ALS-derived height change, we also account for spatial correlation as assessed over stable terrain based on semivariogram analysis (Figure S3) as described in Rolstad et al. (2009). We bias correct the height change over the glacier surfaces using the systematic elevation difference over stable terrain ($\text{Bias}_{\Delta h}$) 250 in the Δ DEMs (Table S3). This bias correction ranged from -0.09–0.05 m and averaged -0.01 m. NMAD reveals random errors that are typically below ± 0.3 m, with a maximum of 0.6 m (Table 3). This maximum error occurred for Zillmer Glacier in late summer 2017 when the separation between site visit and ALS survey was large and new snow covered the glacier during the ALS survey (Table 2).

255 Random uncertainty stems from three sources that we assume to be independent: i) elevation change uncertainty ($\sigma h_{\Delta DEM}$), ii) glacier zone delineation uncertainty (σA), and iii) volume to mass density conversion uncertainty ($\sigma \rho$). We define elevation change uncertainty ($\sigma h_{\Delta DEM}$) following the methods detailed in (Menounos et al., 2018), and found an average decorrelation

length of 0.75 km (Figure S3). Below, we have abbreviated our geodetic and glaciological uncertainty assessment (detailed version: S2)

For delineation of ice/firn/snow zones from satellite imagery (Figure S1), we applied a buffering method (Granshaw and Fountain, 2006) to the perimeter of each zone that was not at the glacier boundary. Our satellite imagery resolution varied from

260 3 to 15 m, so we chose a buffer of four times the largest pixel size to derive an uncertainty in area per zone. This 60 m buffer accounts for uncertainty in zone delineation and changes in the positions of the zone boundaries occurring between ALS and satellite imagery acquisition dates. Total random uncertainty in volume change is:

$$\sigma\Delta V = \sqrt{(\sigma h_{\Delta DEM}(p + 5(1 - p))A)^2 + (\sigma A \cdot h_{\Delta DEM})^2} \quad (3)$$

where A is the area of a given glacier and p is the percentage of surveyed area, which averaged 99.1% (Table 2). Random

265 uncertainty on geodetic mass balance is:

$$\sigma\Delta M = \sum_i \sqrt{(\sigma\Delta V_i \cdot \rho_i)^2 + (\sigma\rho_i \cdot \Delta V)^2} \cdot \frac{A_i}{A_{tot}} \quad (4)$$

where ρ_i is individual density conversion values with associated uncertainties ($\pm\sigma\rho_i$) for spring snow, late summer snow, firn, and ice (Table 4). Prior to being summed to produce a final uncertainty, each zone (ice/firn/snow) is considered separately for B_a , with ΔV_i and A_i the volume and area change of each zone respectively.

270 Firn compaction or fresh snow on the surveyed surface introduce systematic uncertainty on geodetic balance. On Drangajökull ice cap, where B_w is more than 1 m w.e. greater than our average B_w , firn compaction and fresh snow densification increased geodetic B_w by 8%. Fresh snow off-glacier was negligible in all but a few cases. We thus assume a systematic uncertainty ($\sigma\Delta M_{sys}$) of 10% on $B_{a,w}$. Collectively, random and systematic uncertainty thus yield total uncertainty in mass balance:

$$\sigma B_{geod} = \sqrt{(\sigma\Delta M)^2 + (\sigma\Delta M_{sys})^2} \quad (5)$$

275 To determine uncertainty in glaciological mass balance, we derive a mean density (ρ) of mass change (Table 3) and uncertainty in height change for both observations and GPS survey corrections. Uncertainty in glaciological mass balance is calculated as:

$$\sigma B_{a,w} = \sqrt{\sigma\Delta h_{glac}^2 \cdot \rho^2 + \sigma\rho^2 \cdot B_{a,w}^2} \quad (6)$$

where $\sigma\rho$ is the uncertainty on density taken to be 10% of ρ , to account for uncertainty in density measurements and extrapolation of those measurements. The uncertainty in extrapolation of glaciological observations to glacier-wide mass

280 balance is taken as the σ of the different calculations of mass balance for each season.

For both geodetic and glaciological mass balance, B_s was derived as the difference of annual and summer balance (Eqn. 1), and thus uncertainty on B_s yields:

$$\sigma B_s = \sqrt{\sigma B_a^2 + \sigma B_w^2} \quad (7)$$

3 Results

285 3.1 Glaciological Versus Geodetic Balance

Comparison of seasonal balance from glaciological and geodetic methods showed strong overall agreement (Figure 5), with glaciological winter balance (B_{w_glac}) averaging 1.95 ± 0.08 m w.e., 4% greater than our geodetic estimate. Average B_{s_glac} and B_{a_glac} were 3% both more negative than B_{s_geod} and B_{a_geod} (Figure 6). For individual glaciers, average difference between B_{a_glac} and B_{a_geod} was in excellent agreement (-0.03 m w.e. relative to B_{a_glac}), with an average absolute deviation of 0.10 ± 0.07 m w.e. a^{-1} between estimates (Figure 6). B_{w_glac} was 5% greater relative to B_{w_geod} , and B_{s_glac} was 4% more positive relative to B_{s_geod} when considering individual glaciers. For B_w and B_s , geodetic and glaciological balance were within 20% for over 85% of cases. Average mean annual balance from 2015–2017 was -0.73 ± 0.15 m w.e. and -0.76 ± 0.16 m w.e. for glaciological and geodetic methods respectively (Table 3). Mean B_{s_glac} was -2.67 ± 0.13 m w.e. All individual estimates of seasonal and annual balance are within 2σ uncertainties, and only in three instances are they outside 1σ uncertainties (Figure 6).

295 We created a Δ DEM from the first and last late summer DEM for each site (Figure 7) and compared calculated mass change from this Δ DEM to the sum of the individual balance years that comprised that given period (Figure 8). We found that all cumulative seasonal B_a estimates from glaciological and geodetic balance were within uncertainty (2σ) of the last-first mass change approach (Figure 8). Glaciological balance was in net more positive (average $+0.09$ m w.e.) and had an average absolute difference of ± 0.20 m w.e. from the last-first Δ DEM. Summed B_{a_geod} agree with our last-first estimates, with an average 300 deviation of only 0.03 m w.e.

3.2. Glaciological density observations

Glacier averaged snow density from snow pits and cores for spring is 457 ± 48 kg m $^{-3}$, with a coefficient of variation (CV) of 0.14 (n=74). This estimate is 13 kg m $^{-3}$ less than our snow survey based geodetic ρ_{spring} but is within uncertainty (Table 4). For Haig Glacier, average spring density is 420 ± 45 kg m $^{-3}$, 20 kg m $^{-3}$ lighter than our estimate obtained from nearby snow survey 305 measurements, but again within uncertainty. Our average late summer glaciological density of 570 ± 20 kg m $^{-3}$ (n=27) ranged from 536 to 617 kg m $^{-3}$ (CV=0.04). Assigned geodetic ρ_{snow} is 18 kg m $^{-3}$ greater than observations. Average probe depth for spring is 4.20 ± 0.06 m, with a CV of 0.33 (n=1,754). Average probe depth in late summer is 1.85 ± 0.10 m, with a CV of 0.78 (n=777). Observed glacier-wide average snow depths are between 3.4 and 6.9 m, and average 4.56 ± 0.21 m. While spring snow density showed greater variability than late summer snow density, snow depth is far more variable than snow density in 310 both seasons.

Over the period 2015–2017 average AAR was 38% (Table 3), with multi-year firn exposed over 13% of the glacier surface, thus leaving the remaining 49% of glacier area as bare ice. Located in the Rocky Mountains, Haig Glacier is the easternmost site in our study and is in a lower accumulation environment. It has lost nearly all its firn cover over the last 20 years, with firn area at 6% in 2015. The study glaciers that lie in the Columbia Mountains had an AAR of 45% with 15% exposed multi-year 315 firn cover and 40% bare glacier ice.

3.2.1 Geodetic density sensitivity

The effect of using a regional literature-based late summer snow density (Table 5) versus our glaciological density values (Table S1) depends on the amount of retained snow and glaciological density but produces a < 0.01 m w.e. decrease on average, a negligible contribution. Varying firn density by $\pm 15\%$ also has an average effect of ± 0.01 m w.e., with the largest impact

320 a given area of glacier surface has a significant impact, as ρ_{firn} is 17% greater than snow and 26% less than ρ_{ice} . If we produce a single glacier-wide density (ρ) instead of distributing density based on surface classification, we change absolute magnitudes of $B_{a\text{-geod}}$ by an average of ± 0.10 m w.e. Though we did not use it for mass conversion, our ρ of $B_{a\text{-geod}}$ ranged from 681 (Kokanee 2016) to 895 kg m⁻³ (Haig 2017) and averaged 748 ± 61 kg m⁻³.

325 Applying our snow survey density values for spring snow (Table 4) versus our glaciological snow density observations (Table S1) reduces average $B_{w\text{-geod}}$ by 0.03 m w.e. (1.7%) and causes $B_{w\text{-geod}}$ to be from 7% greater rather than 5% relative to $B_{w\text{-glac}}$. For individual glaciers, $B_{w\text{-geod}}$ values between the two methods differ by 1 to 13%, but only 2% on average.

3.3 Glaciological and Geodetic Balance Discrepancies

Estimates of seasonal and annual balance for individual glaciers were outside 1σ uncertainties in a few cases. Conrad $B_{w\text{-glac}}$ 330 was 24% greater than $B_{w\text{-geod}}$ in 2016. Snow accumulation may have occurred in the eight days between the Conrad Glacier ALS survey and field visit, as we observed over 1 m of fresh snow over four days during that interval while on Kokanee Glacier. Automatic snow weather stations near both glaciers at around 2050 m asl showed no accumulation, highlighting the steep balance gradient of the Columbia Mountains. Additionally, ALS acquisition failed over the terminus of the Conrad and Illecillewaet Glaciers in late summer 2015 (Table 2), and our extrapolation based upon the typical gradient over the terminus 335 may have underestimated melt (Figure 7). Kokanee Glacier $B_{a\text{-glac}}$ in 2017 was 0.25 m w.e. more positive than $B_{a\text{-geod}}$, likely due to the burial of a few ablation stakes, and subfreezing temperatures which limited our ability to take adequate snow measurements. Illecillewaet Glacier $B_{w\text{-glac}}$ in 2017 was 46% higher than $B_{w\text{-geod}}$, but this difference may stem from limited $B_{w\text{-glac}}$ observations that year (n=3).

3.4 Interannual and spatial variability

340 Varied climatological conditions provided a range of balance outcomes for the period of study. The lowest $B_{w\text{-glac}}$ of the four studied winters (1.81 ± 0.12 m w.e.) occurred in 2016, yet also the least mass loss with an average $B_{a\text{-glac}}$ of -0.36 ± 0.17 m w.e. (Figure 5). The 2016–2017 winter brought the greatest snowpack of our study period, 2.08 ± 0.18 m w.e., yet substantial mass loss was observed (average $B_{a\text{-glac}}$: -0.84 ± 0.23 m w.e.). The balance year of 2014–2015 saw high sustained mass loss (average $B_{a\text{-glac}}$ of -1.30 ± 0.13 m w.e.), despite having an $B_{w\text{-glac}}$ within 0.01 m w.e. of 2016.

345 The standard deviation between the seasonal and annual balances for each glacier reveals that B_w ($\sigma = 0.14$ m w.e., 7%) experiences lower interannual variability than B_s ($\sigma = 0.38$ m w.e., 14%) and B_a ($\sigma = 0.35$ m w.e., 56%). Kokanee Glacier

experienced the highest B_w in all four years 2015–2018 averaging 2.34 ± 0.30 m w.e. (Figure 6), while Haig Glacier B_w was lowest, averaging 1.37 ± 0.11 m w.e., coupled with the highest mass loss (average B_{a_glac} : -1.62 ± 0.34 m w.e.).

We did not investigate the influence of crevasses for each glacier and each season, but for a test case for each glacier (n=6) we 350 created DEMs with filled crevasses in the late summer, and then produced a Δ DEM. We found that crevasse-free Δ DEM B_w was on average <1% smaller than our standard B_w , with discrepancies up to -0.05 m w.e or -3%. The amount of crevassing is important, however, as some of the studied glaciers such as the Zillmer, Nordic and Conrad feature large crevasse fields.

4 Discussion

The consistency between our geodetic and glaciological seasonal balance estimates among six glaciers over multiple years 355 implies that high-resolution geodetic surveys can be used to reliably measure both winter and summer mass balance. Our study builds upon previous work that established the feasibility of geodetic methods to accurately produce B_w (Belart et al., 2017; Sold et al., 2013), and B_a (Klug et al., 2018). While others show that geodetic surveys can be applied for a single winter (Belart et al., 2017; Sold et al., 2013) or for one glacier over a number of years (Klug et al., 2018), our study demonstrates remotely measured seasonal balance is possible for widely varying rates of accumulation and ablation for multiple glaciers across entire 360 mountain ranges.

4.1 Geodetic seasonal Balance

Our small estimate of $\sigma h_{\Delta DEM}$ (Table S3) and bias correction (Table 3) highlight that height change uncertainty is generally minor, but is important to quantify (Joerg et al., 2012; Klug et al., 2018). As described below, density distribution and conversion factors comprise a large portion of total mass change uncertainty, with firn compaction, fresh snow at the time of 365 ALS acquisition, and crevasses also contributing.

The spatial coverage of ALS is superior to glaciological observations; however, isolating the mass change component of surface height change at a given location is difficult and requires detailed input data (Belart et al., 2017; Sold et al., 2013). While we can develop balance gradients from glaciological data, we have not attempted to do so using our ALS data. To date, studies have differenced their glaciological and geodetic data regarding surface height change and assigned the difference as 370 a combination of vertical ice velocity and firn compaction (Beedle et al., 2014; Belart et al., 2017; Sold et al., 2013) or used full-Stokes ice flow model with a bedrock DEM, a surface DEM, and in situ GPS velocities as inputs (Belart et al., 2017). Then, after applying a simple firn model, vertical ice velocity is estimated. While this method appears robust, and differencing of our glaciological observations of height change from our Δ DEMs produces realistic emergence/submergence velocities, it is beyond the scope of this study.

375 4.1.1 Density distribution and conversion factors

Converting volume to mass change is a major challenge for geodetic studies (Huss, 2013; Moholdt et al., 2010). Over multiple years to decades, a constant value of density can produce tolerable uncertainty of mass change (Huss, 2013). For shorter

timescales, and particularly for seasonal balance, a careful consideration of density is necessary (Klug et al., 2018). Klug et al (2018) used ALS intensity data and satellite imagery for a pixel-based classification of the glacier surface as firn and ice. Our 380 study built on this work and mapped areas of ice, but also distinguished between snow and firn. To investigate the influence of density assumptions, we compare using independent estimates of density and our glaciological data to inform our geodetic estimates, to better constrain the uncertainty on, and compare against, glaciological seasonal balance. Varying the density assigned to each surface class to the maximum and minimum values within our conservative uncertainties has minor effect on 385 seasonal balance but failing to distribute them appropriately has a large impact. If a single density value is used, the range of values of ρ of B_{a_geod} indicates that $750 \pm 60 \text{ kg m}^{-3}$ would be most appropriate for seasonal mass change over this period (Table 3). Given the spread of ρ between glaciers, however, a glacier-specific ρ would be best.

Like Klug et al. (2018), our applied firn density was selected based on a core from a temperate glacier in the Alps (Ambach et al., 1966), and our in situ density measurements for firn ≥ 2 years old matched this value (Table 4). Our glaciological density values for one-year-old firn and late summer snow density are respectively 13.1 and 22.4% (Table 4) less than the assumed 390 value of 700 kg m^{-3} for both snow and firn taken by Klug et al. (2018). Had we also combined snow and firn density, we would have biased B_{a_geod} by varying magnitudes depending upon the surface cover. As glacier mass loss rates continue to accelerate (Menounos et al., 2018), it is reasonable to expect more and older exposed firn during the ablation season, which for geodetic studies, may imply a higher density conversion factor for firn.

Applying glaciological late summer snow density versus our independent regional average density (Table 5) had little effect 395 on B_{a_geod} . Future geodetic studies should use the best available local data, however, as different regions and mountain ranges have different late summer densities (Table 5).

Using our glaciological winter density values to produce B_{w_geod} estimates resulted in a slightly greater discrepancy relative to B_{w_glac} than applying our snow survey-based densities (Table 3). The two B_{w_geod} estimates produced similar results in net, and only a 2% average difference between B_{w_geod} estimates for individual glaciers. In the Columbia and Rocky Mountains, the 400 first significant warming event of the spring typically occurs between early April and early May (Marshall, 2012). Springtime warming tends to homogenize and increase snow density (Adams, 1976; Elder et al., 1991). Our linear regression approach (Figure 3) to adjust glaciological observations of spring snow density (Table S1), appears suitable over the period mid-April through late-May, but we caution against its use for other periods of the year when densification is far slower and less predictable. For Haig Glacier, a linear relation also exists between mid-April through late May (Marshall, 2012, p.18, Fig. 405 2.3). The tendency for a more homogenous snow density, and lack of a consistent altitudinal trend both lend credence to using a single snow density (Fausto et al., 2018; McGrath et al., 2018).

4.1.2 Firn and internal processes

While firn compaction is only incorporated in our uncertainty analysis, others estimate its effect to derive B_{w_geod} (Belart et al., 2017; Sold et al., 2013), but not B_{a_geod} (Klug et al., 2018). For B_{w_geod} , firn compaction was estimated based upon the annual 410 balance in the accumulation zone over a decade (Sold et al., 2013) or over a single balance year (Belart et al., 2017). Currently

accumulation areas on alpine glaciers are in constant flux, are typically discontinuous. Exposed firn is common (Figure S1), implying that the firn zone on our study sites is shrinking in area and thickness, interrupting the cycle of firnification, and invalidating firnification models which assume that one annual layer is transformed from snow to ice annually. Nevertheless, a carefully considered treatment of firn could improve seasonal geodetic balance estimates, but as demonstrated by Belart et al. (2017), firn and fresh snow densification have little effect on B_{w_geod} if the magnitude of winter accumulation is large. For regions with low winter balance, or a colder climate, compaction would have a larger relative influence on B_w .

Meltwater retention is not incorporated into our annual balance estimates. At Haig Glacier, firn meltwater retention has not been measured, but meltwater retention in the supraglacial snowpack is a negligible contributor to mass balance, though it does create an effective “energy sink”, that should be accounted for in mass balance modeling (Samimi and Marshall, 2017).

For glaciers in Svalbard, coupled energy balance and snow/hydrology models have been used to quantify the effects of meltwater freezing and retention on glacier mass balance (Van Pelt et al., 2012; Van Pelt and Kohler, 2015). Rates of meltwater retention are decreasing for Svalbard glaciers (Van Pelt and Kohler, 2015), and on the Devon Ice Cap (Bezeau et al., 2013), due to decreasing firn area and in particular, warmer temperature. Like at our glaciers, melt-freeze cycles form thick ‘summer surface’ layers on these Svalbard glaciers and Devon Ice Cap, which could act as a barrier for vertical water transport and is likely to promote near-surface lateral water flow, limiting deep firn water storage (Gascon et al., 2013; Van Pelt and Kohler, 2015).

Geodetic balance implicitly includes internal and basal mass change, which are not captured by the glaciological method. Studies of these processes are rare and are based upon estimates rather than verified measurements. Estimates of annual mass loss from geothermal heat, potential energy released by runoff or ice motion, and basal friction are typically around 0.01 to 0.10 m w.e. (Huss et al., 2009; Oerlemans, 2013; Sold et al., 2016). Crevasses and internal processes likely combine to be 0 to 4% of the magnitude of average annual ablation (e.g. Klug et al., 2018; Sold et al., 2016), and thus are likely not major contributors to seasonal balance in the Columbia Mountains. Modeled meltwater accumulation in firn would tend to increase mass balance, possibly offsetting typical basal/internal mass loss, but would not be captured by geodetic or glaciological measurements. Most mass balance models only assume vertical percolation of meltwater yet given thick impermeable ice layers observed in our cores and snow pits, and in other studies (Gascon et al., 2013; Van Pelt and Kohler, 2015), this assumption would lead to an overestimation of refreezing. Without regional data to constrain firn processes it is difficult to incorporate them into mass balance calculations. Regionally, a better understanding of firn processes could improve annual balance and runoff estimates, and likely has a greater influence on the large icefields in western North America, which have received little attention. Although firn processes are not resolved, our approach markedly improves the quality of annual results compared to calculations based on a fixed glacier-wide conversion density.

4.1.3 Fresh snow

Presence of fresh snow at the time of acquisition is a challenge for any geodetic survey estimating mass change (Belart et al., 2017; Joerg et al., 2012; Klug et al., 2018). Fresh snow can change the height of the target surface by tens of centimeters. Our

bias correction of Δ DEM height change (Figure S2, Table 3) corrected for small quantities of fresh snow, assuming that snow
445 was present over stable terrain. In late summer, we could detect fresh snow visually, as a hillshade of the glacier surface at 1 m resolution captures intricate details which are easily disguised by snow depths of 0.2 m or more. Off-glacier, the depth and distribution of fresh snow is variable due to redistribution and the thermal properties of bedrock and other surfaces. In spring, we are unable to detect fresh snow as the only snow-free pixels in our scenes are typically rock faces with extreme slopes and tree tops. Our $\sigma\Delta M_{sys}$ attempts to approximate the systematic uncertainty introduced by fresh snow and firn compaction.

450 4.1.4 Crevasses

Crevasses can affect both B_{w_geod} and B_{w_glac} since crevasses bridged by winter snowpack will overestimate B_{w_geod} snow volume, and crevasses filled by snow would not be captured by B_{w_glac} . We produced ‘crevasse-free’ glacier surfaces by resampling late summer DEMs to 10 m using the maximum elevations within the smoothing window to avoid in-crevasse height measurements. Using the 10 m ‘crevasse-free’ DEMs versus the original 1 m DEMs had little influence on B_{w_geod} , with
455 only the Zillmer and Nordic glaciers showing a difference >1%. We did not extend these test cases to cover B_{a_geod} estimates because the area of exposed crevasses varied little year to year. On Hintereisferner, crevasse effects biased B_{a_geod} by only 0.03% (-0.047 m w.e.) over a decade (Klug et al., 2018). Despite the small influence of crevassing on B_{a_geod} observed in this study, additional studies should quantify the magnitude of this bias in greater detail.

4.2 Glaciological seasonal balance

460 Observational biases include the representativeness of sampling sites and number of measurements (Cogley, 1999; Fountain and Vecchia, 1999), and the extrapolation of those measurements to produce a glacier-wide balance estimate (Sold et al., 2016; Thibert and Vincent, 2009). The difficulty of comparability between methods and sites (Cogley, 1999; Fountain and Vecchia, 1999) is an ongoing challenge due to logistical and financial obstacles to in situ mass balance studies. Areas of a glacier may be inaccessible, and preferred paths chosen for measurement may be biased to areas which better retain snowpack for safety
465 purposes (Østrem and Brugman, 1991).

4.2.1 Snow depth

We observed best agreement between geodetic and glaciological measurements of winter balance during years of dense field surveys. Safety or logistical constraints prevented us from completing all transects of snow depth measurements in some years, with greater discrepancies between estimates in cases with incomplete coverage. In both spring and late summer, we
470 encountered internal ice layers at some or all sites. Ice lenses were most common in the accumulation zone, but they were also found in the ablation zone in spring. These internal layers form via rain-on-snow events (McCabe et al., 2007) or, as the melt season progresses, via internal storage of meltwater (Pfeffer and Humphrey, 1996). Ice layers 2–6 cm thick were present nearly every year in the accumulation zone of the Conrad Glacier, and often at other sites. We were able to penetrate these layers and

successfully measure spring snow depth using our industrial avalanche probe. A conventional avalanche probe is unsuitable
475 for glaciological observations in the Columbia Mountains.

The greater B_{w_geod} of 2016 on Conrad Glacier is likely due to both snow accumulation between the glaciological visit and
475 ALS survey, and to the late summer 2015 ALS survey missing the lowest reaches of the glacier, preventing calculation of
surface height change for that portion of the glacier. We estimated the snow depth for the lower reaches of the glacier based
480 upon the ratio of snow depth observed there for other years relative to the rest of glacier, and snow depths along the cut-off
margin. The B_w discrepancy for Zillmer Glacier in 2016 is likely due to glaciological sampling bias, as the east transect (Figure
485 4), which has a lesser snowpack, was not sampled, and the 30 day difference between field and ALS survey date (Table 2)
may not be adequately resolved by the GPS survey correction.

4.2.2 Mass change between measurements

Previous studies account for mass change that occurs between measurements by using a distributed temperature index model
485 (Sold et al., 2013) or degree-day model (Belart et al., 2017), but these models do not account for snow gain. We utilized in situ
GPS surveys of the glacier height which were then compared with ALS DEMs. We binned and averaged our height change
estimates by 100 m elevation bands (Figure S5), and then applied a density to each band based on satellite observations of a
given surface class. Limitations in our approach include: 1) fresh snowfall between the GPS and ALS surveys; and 2)
490 significant densification of the snowpack in spring. Terrain presents a further challenge to kinematic GPS survey observations.

The GPS antenna is securely mounted in the backpack of a field member, but the measured height of the antenna above the
glacier surface may vary due to the uneven glacier terrain, particularly during travel on steep slopes (Beedle et al., 2014).

Our median dates of late summer glaciological visits and geodetic surveys are September 6th, and September 18th respectively
(Table 2). Snowfall can occur at any time of the year in the Columbia and Rocky Mountains (Schnorbus et al., 2014), and in
late August, throughout September, and even into early October, either melt or accumulation can prevail (Marshall, 2014).

495 Lowering of the surface via ablation post ALS survey dates (Table 2) is not accounted for and would cause an underestimated
winter snowpack. While our methods are comparable year-to-year, and between sites, our B_w and B_s values are not the total
amount of snow and runoff during a year. We do not include snow which falls between May and August and melts off and
cannot measure ablation occurring after our ALS survey or glaciological visit, whichever occurs later. Thus, our B_w and B_s
values represent a conservative estimate of runoff contributions from snow and ice melt.

500 5. Conclusions

Estimates of seasonal mass balance presented here show strong agreement between glaciological and geodetic methods for
individual glaciers, and are within 1σ uncertainties for average winter, summer, and annual balance. These independent
estimates of seasonal mass change  over three years from glaciers separated by hundreds of kilometers. Our findings
505 suggest that high-resolution geodetic methods, such as from ALS (Klug et al., 2018; Sold et al., 2013), aerial photogrammetry
(Nolan et al., 2015), and stereo satellite imagery (Belart et al., 2017; Berthier et al., 2014) can be used to produce accurate

seasonal and annual balance estimates over large areas. The quality of geodetic annual balance estimates depends more on distributing density via surface classification (Klug et al., 2018), than on the density values themselves. The spatial coverage, density of observations, and measurement precision of high-resolution geodetic terrain analysis compensates for uncertainty associated with fresh snow and firn compaction, internal and basal mass change, and crevasses (Belart et al., 2017; Klug et al., 510 2018). The minimal impact of these factors on mass balance stems from the large mass changes observed at our sites, as reported elsewhere (Belart et al., 2017; Klug et al., 2018). For glaciers with low mass turnover, errors introduced by firn compaction, crevasses, and fresh snow may be considerably larger than observed in our study, however. 

Our estimate of spring snow density for geodetic measurements from provincial snow survey observations (Figure 2) is within the uncertainty of our measured glaciological spring snow density (Table 4). Our approach holds promise for being able to use 515 regional density estimates when in situ measurements are unavailable, yet discrepancies of up to 13% between geodetic and glaciological winter balance estimates indicate the uncertainty introduced when using density values which are not site-specific. Estimates of end-of-season snow density introduce a possible bias, but given the regional consistency of late summer snow density, and the overall lack of a density-altitude gradient in spring, using a single snow density is a robust method for converting snow depth to water equivalence (Fausto et al., 2018; McGrath et al., 2018). We observed greater variability in B_s 520 relative to B_w , highlighting the need for models of glacier mass balance that can be able to reliably reproduce widely varying rates of mass loss corresponding to the multitude of energy fluxes that influence alpine glaciers (Fitzpatrick et al., 2017), to reliably estimate seasonal mass balance.

The hydrologic cycle of western North America is dominated by snowfall in the mountains, but observations of alpine snowpack above 2000 m asl are sparse. As the climate continues to change, there is a growing need for a more detailed 525 understanding of the seasonal balance of glaciers and snowpack. Geodetic methods are needed to supplement in situ observations across many mountain regions in order to address the contribution of glaciers to changes in freshwater runoff availability, and to sea level rise. To date, the majority of high-resolution geodetic balance studies of seasonal or annual balance have been conducted in the European Alps, where extensive, multi-decadal glaciological data are available (Klug et al., 2018; Sold et al., 2013, 2016). Our study suggests that geodetic methods can be used to assess seasonal balance of glaciers, even in 530 mountain ranges lacking long-term records of mass balance, if density is carefully considered (Belart et al., 2017; Klug et al., 2018). Recent advances in satellite technology (Berthier et al., 2014; Marti et al., 2016) suggest that such efforts can be made with increasing spatial and temporal coverage, greatly adding to our understanding of the seasonal contribution of snow and glaciers to mountain hydrology. 

Acknowledgements

535 We acknowledge financial support from the Columbia Basin Trust, BC Hydro, the Pacific Institute for Climate Solutions, the Natural Resources and Engineering Research Council of Canada, the Canada Chairs Program, and the Tula Foundation. B. Pelto conducted the field work with the help of many invaluable volunteers, and conducted the bulk of the ALS processing, 



and analysis. Analysis of Haig Glacier was conducted by Shawn Marshall. The authors wish to thank Amaury Dehecq for assistance with DEM coregistration. All glaciological mass balance data will be available through the WGMS. All authors contributed to the writing of the manuscript. The authors declare that they have no conflict of interest.

References

Abermann, J., Fischer, A., Lambrecht, A. and Geist, T.: On the potential of very high-resolution repeat DEMs in glacial and periglacial environments, *The Cryosphere*, 4(1), 53, 2010.

Adams, W.: Areal differentiation of snow cover in east central Ontario, *Water Resour. Res.*, 12(6), 1226–1234, 1976.

545 Ambach, W., Bortenschlager, S. and Eisner, H.: Pollen-analysis investigation of a 20 m. Firn Pit on the Kesselwandferner (Ötztal Alps), *J. Glaciol.*, 6(44), 233–236, 1966.

Barnett, T. P., Adam, J. C. and Lettenmaier, D. P.: Potential impacts of a warming climate on water availability in snow-dominated regions, *Nature*, 438(7066), 303–309, doi:10.1038/nature04141, 2005.

550 Beedle, M. J., Menounos, B. and Wheate, R.: An evaluation of mass-balance methods applied to Castle Creek Glacier, British Columbia, Canada, *J. Glaciol.*, 60(220), 262–276, doi:10.3189/2014JoG13J091, 2014.

Belart, J. M. C., Berthier, E., Magnússon, E., Anderson, L. S., Pálsson, F., Thorsteinsson, T., Howat, I. M., Aðalgeirsdóttir, G., Jóhannesson, T. and Jarosch, A. H.: Winter mass balance of Drangajökull ice cap (NW Iceland) derived from satellite sub-meter stereo images, *The Cryosphere*, 11(3), 1501–1517, doi:10.5194/tc-11-1501-2017, 2017.

555 Benson, C. S.: Stratigraphic studies in the snow and firn of the Greenland ice sheet, *Cold Regions Research and Engineering Lab Hanover NH.*, 1962.

Berthier, E., Vincent, C., Magnússon, E., Gunnlaugsson, Á., Pitte, P., Le Meur, E., Masiokas, M., Ruiz, L., Pálsson, F. and Belart, J.: Glacier topography and elevation changes derived from Pléiades sub-meter stereo images, *Cryosphere*, 8(6), 2275–2291, 2014.

560 Bevington, A., Gleason, H., Giroux-Bougard, X. and de Jong, J. T.: A Review of Free Optical Satellite Imagery for Watershed-Scale Landscape Analysis, *Conflu. J. Watershed Sci. Manag.*, 2(2), 2018.

Bezeau, P., Sharp, M., Burgess, D. and Gascon, G.: Firn profile changes in response to extreme 21st-century melting at Devon Ice Cap, Nunavut, Canada, *J. Glaciol.*, 59(217), 981–991, 2013.

Bolch, T., Menounos, B. and Wheate, R.: Landsat-based inventory of glaciers in western Canada, 1985–2005, *Remote Sens. Environ.*, 114(1), 127–137, doi:10.1016/j.rse.2009.08.015, 2010.

565 Bollmann, E., Sailer, R., Briese, C., Stötter, J. and Fritzmann, P.: Potential of airborne laser scanning for geomorphologic feature and process detection and quantifications in high alpine mountains, *Z. Für Geomorphol. Suppl. Issues*, 55(2), 83–104, 2011.

Brahney, J., Weber, F., Foord, V., Janmaat, J. and Curtis, P. J.: Evidence for a climate-driven hydrologic regime shift in the Canadian Columbia Basin, *Can. Water Resour. Journal/Révue Can. Ressour. Hydr.*, 42(2), 179–192, 2017.

570 Clarke, G. K. C., Anslow, F. S., Jarosch, A. H., Radić, V., Menounos, B., Bolch, T. and Berthier, E.: Ice Volume and Subglacial Topography for Western Canadian Glaciers from Mass Balance Fields, Thinning Rates, and a Bed Stress Model, *J. Clim.*, 26(12), 4282–4303, doi:10.1175/JCLI-D-12-00513.1, 2013.

Clarke, G. K. C., Jarosch, A. H., Anslow, F. S., Radić, V. and Menounos, B.: Projected deglaciation of western Canada in the twenty-first century, *Nat. Geosci.*, doi:10.1038/ngeo2407, 2015.

575 Cogley, J., Hock, R., Rasmussen, L., Arendt, A., Bauder, A., Braithwaite, R., Jansson, P., Kaser, G., Möller, M. and Nicholson, L.: Glossary of glacier mass balance and related terms, IHP-VII technical documents in hydrology No. 86, IACS Contribution No. 2, Int. Hydrol. Program UNESCO Paris, 2011.

Cogley, J. G.: Effective sample size for glacier mass balance, *Geogr. Ann. Ser. Phys. Geogr.*, 81(4), 497–507, 1999.

580 Cohen, S. J., Miller, K. A., Hamlet, A. F. and Avis, W.: Climate change and resource management in the Columbia River Basin, *Water Int.*, 25(2), 253–272, 2000.

Conger, S. M. and McClung, D. M.: Comparison of density cutters for snow profile observations, *J. Glaciol.*, 55(189), 163–169, 2009.

Cuffey, K. M. and Paterson, W. S. B.: *The physics of glaciers*, Academic Press., 2010.

585 Dadic, R., Mott, R., Lehning, M. and Burlando, P.: Wind influence on snow depth distribution and accumulation over glaciers, *J. Geophys. Res.*, 115(F1), doi:10.1029/2009JF001261, 2010.

Demarchi, D. A.: An introduction to the ecoregions of British Columbia., 2011.

Elder, K., Dozier, J. and Michaelsen, J.: Snow accumulation and distribution in an alpine watershed, *Water Resour. Res.*, 27(7), 1541–1552, 1991.

590 Environment Canada: Canadian Climate Normals, Gov. Can. [online] Available from: http://climate.weather.gc.ca/climate_normals/index_e.html, 2019.

Escher-Vetter, H., Kuhn, M. and Weber, M.: Four decades of winter mass balance of Vernagtferner and Hintereisferner, Austria: methodology and results, *Ann. Glaciol.*, 50(50), 87–95, doi:10.3189/172756409787769672, 2009.

595 Fausto, R. S., Box, J. E., Vandecrux, B., van As, D., Steffen, K., MacFerrin, M. J., Machguth, H., Colgan, W., Koenig, L. S., McGrath, D., Charalampidis, C. and Braithwaite, R. J.: A Snow Density Dataset for Improving Surface Boundary Conditions in Greenland Ice Sheet Firn Modeling, *Front. Earth Sci.*, 6, 51, doi:10.3389/feart.2018.00051, 2018.

Fischer, A.: Comparison of direct and geodetic mass balances on a multi-annual time scale, *The Cryosphere*, 5(1), 107–124, doi:10.5194/tc-5-107-2011, 2011.

Fitzpatrick, N., Radić, V. and Menounos, B.: Surface Energy Balance Closure and Turbulent Flux Parameterization on a Mid-Latitude Mountain Glacier, Purcell Mountains, Canada, *Front. Earth Sci.*, 5, 67, 2017.

600 Fountain, A. G. and Vecchia, A.: How many stakes are required to measure the mass balance of a glacier?, *Geogr. Ann. Ser. Phys. Geogr.*, 81(4), 563–573, 1999.

Gabrielli, P., Carturan, L., Gabrieli, J., Dinale, R., Krainer, K., Hausmann, H., Davis, M., Zagorodnov, V., Seppi, R., Barbante, C., Dalla Fontana, G. and Thompson, L. G.: Atmospheric warming threatens the untapped glacial archive of Ortles mountain, South Tyrol, *J. Glaciol.*, 56(199), 843–853, doi:10.3189/002214310794457263, 2010.

605 Gascon, G., Sharp, M., Burgess, D., Bezeau, P. and Bush, A. B.: Changes in accumulation-area firn stratigraphy and meltwater flow during a period of climate warming: Devon Ice Cap, Nunavut, Canada, *J. Geophys. Res. Earth Surf.*, 118(4), 2380–2391, 2013.

Granshaw, F. D. and Fountain, A. G.: Glacier change (1958–1998) in the north Cascades national park complex, Washington, USA, *J. Glaciol.*, 52(177), 251–256, 2006.

610 Hamlet, A. F. and Lettenmaier, D. P.: Columbia River streamflow forecasting based on ENSO and PDO climate signals, *J. Water Resour. Plan. Manag.*, 125(6), 333–341, 1999.

Hamlet, A. F., Mote, P. W., Clark, M. P. and Lettenmaier, D. P.: Effects of temperature and precipitation variability on snowpack trends in the Western United States*, *J. Clim.*, 18(21), 4545–4561, 2005.

615 Helffricht, K., Schöber, J., Seiser, B., Fischer, A., Stötter, J. and Kuhn, M.: Snow accumulation of a high alpine catchment derived from LiDAR measurements, *Adv. Geosci.*, 32, 31–39, 2012.

Helffricht, K., Kuhn, M., Keuschnig, M. and Heilig, A.: Lidar snow cover studies on glaciers in the Ötztal Alps (Austria): comparison with snow depths calculated from GPR measurements, *The Cryosphere*, 8(1), 41–57, doi:10.5194/tc-8-41-2014, 2014.

Herron, M. M. and Langway, C. C.: Firn densification: an empirical model, *J. Glaciol.*, 25(93), 373–385, 1980.

620 Hirose, J. M. R. and Marshall, S. J.: Glacier Meltwater Contributions and Glaciometeorological Regime of the Illecillewaet River Basin, British Columbia, Canada, *Atmosphere-Ocean*, 51(4), 416–435, doi:10.1080/07055900.2013.791614, 2013.

Huss, M.: Density assumptions for converting geodetic glacier volume change to mass change, *The Cryosphere*, 7(3), 877–887, doi:10.5194/tc-7-877-2013, 2013.

Huss, M. and Hock, R.: Global-scale hydrological response to future glacier mass loss, *Nat. Clim. Change*, 8(2), 135, 2018.

625 Huss, M., Bauder, A., Funk, M. and Hock, R.: Determination of the seasonal mass balance of four Alpine glaciers since 1865, *J. Geophys. Res.*, 113(F1), doi:10.1029/2007JF000803, 2008.

Joerg, P. C., Morsdorf, F. and Zemp, M.: Uncertainty assessment of multi-temporal airborne laser scanning data: A case study on an Alpine glacier, *Remote Sens. Environ.*, 127, 118–129, doi:10.1016/j.rse.2012.08.012, 2012.

630 Jost, G., Moore, R. D., Menounos, B. and Wheate, R.: Quantifying the contribution of glacier runoff to streamflow in the upper Columbia River Basin, Canada, *Hydrol. Earth Syst. Sci.*, 16(3), 849–860, doi:10.5194/hess-16-849-2012, 2012.

Kääb, A.: Remote sensing of mountain glaciers and permafrost creep, *Geographisches Institut der Universität Zürich*, Zürich., 2005.

Klug, C., Bollmann, E., Galos, S. P., Nicholson, L., Prinz, R., Rieg, L., Sailer, R., Stötter, J. and Kaser, G.: Geodetic reanalysis of annual glaciological mass balances (2001–2011) of Hintereisferner, Austria, *The Cryosphere*, 12(3), 833–849, doi:10.5194/tc-12-833-2018, 2018.

Machguth, H., Eisen, O., Paul, F. and Hoelzle, M.: Strong spatial variability of snow accumulation observed with helicopter-borne GPR on two adjacent Alpine glaciers, *Geophys. Res. Lett.*, 33(13), doi:10.1029/2006GL026576, 2006.

Marshall, S.: *The Cryosphere*, Princeton University Press, Princeton., 2012.

Marshall, S. J.: Meltwater run-off from Haig Glacier, Canadian Rocky Mountains, 2002-2013, *Hydrol. Earth Syst. Sci.*, 18(12), 5181, 2014.

Marti, R., Gascoin, S., Berthier, E., Pinel, M. de, Houet, T. and Laffly, D.: Mapping snow depth in open alpine terrain from stereo satellite imagery, *The Cryosphere*, 10(4), 1361–1380, 2016.

Maussion, F., Butenko, A., Champollion, N., Dusch, M., Eis, J., Fourteau, K., Gregor, P., Jarosch, A. H., Landmann, J. and Oesterle, F.: The Open Global Glacier Model (OGGM) v1. 1, *Geosci. Model Dev.*, 12(3), 909–931, 2019.

645 McCabe, G. J., Hay, L. E. and Clark, M. P.: Rain-on-Snow Events in the Western United States, *Bull. Am. Meteorol. Soc.*, 88(3), 319–328, doi:10.1175/BAMS-88-3-319, 2007.

McGrath, D., Sass, L., O’Neel, S., Arendt, A., Wolken, G., Gusmeroli, A., Kienholz, C. and McNeil, C.: End-of-winter snow depth variability on glaciers in Alaska, *J. Geophys. Res. Earth Surf.*, 120(8), 1530–1550, doi:10.1002/2015JF003539, 2015.

650 McGrath, D., Sass, L., O’Neel, S., McNeil, C., Candela, S. G., Baker, E. H. and Marshall, H.-P.: Interannual snow accumulation variability on glaciers derived from repeat, spatially extensive ground-penetrating radar surveys, *The Cryosphere*, 12(11), 3617–3633, doi:10.5194/tc-12-3617-2018, 2018.

Menounos, B., Hugonnet, R., Shean, D., Gardner, A., Howat, I., Berthier, E., Pelto, B., Tennant, C., Shea, J. and Noh, M.: Heterogeneous changes in western North American glaciers linked to decadal variability in zonal wind strength, *Geophys. Res. Lett.*, 2018.

655 Miller, M. M. and Pelto, M. S.: Mass balance measurements on the Lemon Creek Glacier, Juneau Icefield, Alaska 1953–1998, *Geogr. Ann. Ser. Phys. Geogr.*, 81(4), 671–681, 1999.

Moholdt, G., Nuth, C., Hagen, J. O. and Kohler, J.: Recent elevation changes of Svalbard glaciers derived from ICESat laser altimetry, *Remote Sens. Environ.*, 114(11), 2756–2767, doi:10.1016/j.rse.2010.06.008, 2010.

660 Najafi, M. R., Zwiers, F. and Gillett, N.: Attribution of the Observed Spring Snowpack Decline in British Columbia to Anthropogenic Climate Change, *J. Clim.*, 30(11), 4113–4130, doi:10.1175/JCLI-D-16-0189.1, 2017.

Nolan, M., Larsen, C. and Sturm, M.: Mapping snow depth from manned aircraft on landscape scales at centimeter resolution using structure-from-motion photogrammetry, *The Cryosphere*, 9(4), 1445–1463, doi:10.5194/tc-9-1445-2015, 2015.

665 Oerlemans, J., Anderson, B., Hubbard, A., Huybrechts, P., Johannesson, T., Knap, W. H., Schmeits, M., Stroeve, A. P., Van de Wal, R. S. W., Wallinga, J. and others: Modelling the response of glaciers to climate warming, *Clim. Dyn.*, 14(4), 267–274, 1998.

Ohmura, A.: Observed mass balance of mountain glaciers and Greenland ice sheet in the 20th century and the present trends, *Surv. Geophys.*, 32(4–5), 537–554, 2011.

Østrem, G. and Brugman, M.: Mass balance measurement techniques, *Man. Field Off. Work Natl. Hy-Drology Res. Inst. NHRI Sci. Rep.*, (4), 1991.

670 Pelto, M. S.: Annual net balance of North Cascade glaciers, 1984-94, *J. Glaciol.*, 42(140), 3–9, 1996.

Pelto, M. S.: The current disequilibrium of North Cascade glaciers, *Hydrol. Process.*, 20(4), 769–779, doi:10.1002/hyp.6132, 2006.

Pelto, M. S. and Miller, M. M.: Mass balance of the Taku Glacier, Alaska from 1946 to 1986, *Northwest Sci.*, 64(3), 1990.

Pelto, M. S. and Riedel, J.: Spatial and temporal variations in annual balance of North Cascade glaciers, Washington 1984-675 2000, *Hydrol. Process.*, 15(18), 3461–3472, doi:10.1002/hyp.1042, 2001.

Pelto, M. S., Kavanaugh, J. and McNeil, C.: Juneau icefield mass balance program 1946–2011, *Earth Syst. Sci. Data*, 5(2), 319–330, 2013.

Pfeffer, W. and Humphrey, N.: Determination of timing and location of water movement and ice-layer formation by temperature measurements in sub-freezing snow, *J. Glaciol.*, 42(141), 292–304, 1996.

680 Proksch, M., Rutter, N., Fierz, C. and Schneebeli, M.: Intercomparison of snow density measurements: bias, precision, and vertical resolution, *The Cryosphere*, 10(1), 371–384, 2016.

Pulwicki, A., Flowers, G. E., Radić, V. and Bingham, D.: Estimating winter balance and its uncertainty from direct measurements of snow depth and density on alpine glaciers, *J. Glaciol.*, 1–15, doi:10.1017/jog.2018.68, 2018.

Radić, V. and Hock, R.: Glaciers in the Earth’s Hydrological Cycle: Assessments of Glacier Mass and Runoff Changes on 685 Global and Regional Scales, *Surv. Geophys.*, 35(3), 813–837, doi:10.1007/s10712-013-9262-y, 2014.

Ragettli, S., Immerzeel, W. W. and Pellicciotti, F.: Contrasting climate change impact on river flows from high-altitude catchments in the Himalayan and Andes Mountains, *Proc. Natl. Acad. Sci.*, 113(33), 9222–9227, 2016.

Samimi, S. and Marshall, S. J.: Diurnal Cycles of Meltwater Percolation, Refreezing, and Drainage in the Supraglacial Snowpack of Haig Glacier, Canadian Rocky Mountains, *Front. Earth Sci.*, 5, 6, 2017.

690 Schnorbus, M., Werner, A. and Bennett, K.: Impacts of climate change in three hydrologic regimes in British Columbia, Canada, *Hydrol. Process.*, 28(3), 1170–1189, doi:10.1002/hyp.9661, 2014.

Sinclair, K. and Marshall, S.: Temperature and vapour-trajectory controls on the stable-isotope signal in Canadian Rocky Mountain snowpacks, *J. Glaciol.*, 55(191), 485–498, 2009.

Sold, L., Huss, M., Hoelzle, M., Anderegg, H., Joerg, P. C. and Zemp, M.: Methodological approaches to infer end-of-winter 695 snow distribution on alpine glaciers, *J. Glaciol.*, 59(218), 1047–1059, doi:10.3189/2013JoG13J015, 2013.

Sold, L., Huss, M., Eichler, A., Schwikowski, M. and Hoelzle, M.: Recent accumulation rates of an alpine glacier derived from firn cores and repeated helicopter-borne GPR, *Cryosphere Discuss.*, 8(4), 4431–4462, doi:10.5194/tcd-8-4431-2014, 2014.

Sold, L., Huss, M., Machguth, H., Joerg, P. C., Leysinger Vieli, G., Linsbauer, A., Salzmann, N., Zemp, M. and Hoelzle, M.: 700 Mass balance re-analysis of Findelengletscher, Switzerland; benefits of extensive snow accumulation measurements, *Front. Earth Sci.*, 4, 18, 2016.

Stahl, K. and Moore, R. D.: Influence of watershed glacier coverage on summer streamflow in British Columbia, Canada, *Water Resour. Res.*, 42(6), doi:10.1029/2006WR005022, 2006.

Thibert, E. and Vincent, C.: Best possible estimation of mass balance combining glaciological and geodetic methods, Ann. Glaciol., 50(50), 112–118, 2009.

705 Van Pelt, W. and Kohler, J.: Modelling the long-term mass balance and firn evolution of glaciers around Kongsfjorden, Svalbard, J. Glaciol., 61(228), 731–744, doi:10.3189/2015JoG14J223, 2015.

Van Pelt, W., Oerlemans, J., Reijmer, C., Pohjola, V., Pettersson, R. and Van Angelen, J.: Simulating melt, runoff and refreezing on Nordenskiöldbreen, Svalbard, using a coupled snow and energy balance model, The Cryosphere, 6(3), 641–659, 2012.

710 Weber, F. and Litke, T.: Standard Operating Procedure Maintainence and Sampling Procedure Manual Snow Surveying, BC Hydro., 2018.

WGMS: Fluctuations of Glaciers Database, World Glacier Monit. Serv., doi:10.5904/wgms-fog-2018-11, 2018.

715 **Table 1: Glacier specific details. Firn ratio refers to the area of a glacier covered by multi-year firn, which is the combination of accumulation area and exposed firn from 2015 imagery.**

Glacier	Area (km ²)	Max Elev. (m)	Min Elev. (m)	Range (m)	Mean Elev. (m)	Length (km)	Firn Ratio	Aspect
Zillmer	5.43	2860	1860	1000	2380	5.59	0.59	NW
Nordic	3.39	2990	2065	925	2515	3.30	0.62	N
Illecillewaet	7.72	2908	2147	761	2532	4.29	0.48	WNW
Haig	2.62	2870	2461	409	2660	2.45	0.06	SE
Conrad	11.45	3235	1825	1410	2595	12.18	0.58	N
Kokanee	1.79	2805	2220	585	2585	2.20	0.48	N

Table 2: Date and number of observation locations (n) for glaciological visits and geodetic acquisition dates and point density. Field dates are median date of glacier visit.

Year	Glacier	Autumn Glac.	n	Autumn ALS	Cover (%)	Points m ⁻²	Winter Glac.	n	Winter ALS	Cover (%)	Points m ⁻²
2015	Zillmer	8/23/2015	23	10/3/2015	100	2.75	5/30/2015	20	4/19/2015	100	3.34
2016	Zillmer	8/15/2016	23	9/14/2016	100	2.44	4/14/2016	46	4/18/2016	100	3.69
2017	Zillmer	8/22/2017	26	11/3/2017	100	1.49	4/13/2017	31	5/20/2017	100	0.80
2018	Zillmer	—	—	—	—	—	5/19/2018	42	4/29/2018	100	4.37
2014	Nordic	8/29/2014	8	9/11/2014	100	8.71	4/27/2014	16	—	—	—
2015	Nordic	8/31/2015	11	9/11/2015	99	1.99	5/1/2015	20	4/19/2015	100	3.04
2016	Nordic	8/21/2016	21	9/12/2016	99	3.27	5/2/2016	28	4/17/2016	100	3.21
2017	Nordic	9/14/2017	18	9/27/2017	100	2.35	5/1/2017	21	5/21/2017	100	0.96
2018	Nordic	—	—	—	—	—	5/1/2018	21	4/26/2018	100	1.84
2015	Illecillewaet	9/24/2015	9	9/11/2015	97	1.02	—	—	4/19/2015	100	2.31
2016	Illecillewaet	9/13/2016	7	9/12/2016	100	1.37	—	—	4/17/2016	100	2.50

2017	Illecillewaet	9/27/2017	7	9/17/2017	100	2.59	5/19/2017	3	5/21/2017	100	1.22
2018	Illecillewaet	—	—	—	—	—	—	—	4/26/2018	100	1.64
2015	Haig	9/12/2015	2	9/12/2015	100	0.93	5/12/2015	33	4/20/2015	100	2.89
2016	Haig	9/13/2016	1	9/13/2016	100	1.85	5/18/2016	33	4/17/2016	100	2.64
2017	Haig	9/16/2017	1	9/16/2017	97	4.82	5/12/2017	33	5/21/2017	100	1.09
2018	Haig	—	—	—	—	—	—	—	4/27/2018	100	3.23
2014	Conrad	9/4/2014	7	9/11/2014	100	10.38	—	—	—	—	—
2015	Conrad	9/5/2015	9	9/12/2015	92	1.35	4/23/2015	38	4/20/2015	100	3.58
2016	Conrad	8/28/2016	31	9/12/2016	100	2.45	4/26/2016	44	4/17/2016	100	2.45
2017	Conrad	9/10/2017	42	9/17/2017	94	3.70	5/15/2017	59	5/21/2017	100	1.29
2018	Conrad	—	—	—	—	—	4/24/2018	56	4/26/2018	100	1.84
2015	Kokanee	8/27/2015	11	9/12/2015	100	1.04	4/20/2015	20	4/19/2015	100	2.99
2016	Kokanee	9/5/2016	23	9/13/2016	100	2.07	4/19/2016	33	4/17/2016	100	2.77
2017	Kokanee	9/19/2017	15	9/16/2017	83	2.63	4/17/2017	23	5/21/2017	100	0.92
2018	Kokanee	—	—	—	—	—	4/18/2018	21	4/26/2018	100	1.33

720

Table 3: Seasonal balance and uncertainty estimates for geodetic (geod) and glaciological mass balance (glac) in m w.e. Kinematic GPS survey-derived corrections applied to glaciological data (surv.corr). Statistical analysis of the DEMs over stable terrain include NMAD, median height difference, and bias correction applied over the glacier (Bias_{Δh}). Mean density of Ba_{geod} is $\bar{\rho}$.

Average values include only cases where both geodetic and glaciologic data were collected. Bw_{geod,gl} is calculated using glaciological densities (Table S1), and Bw_{geod,ss} is calculated using snow survey data (Figure 2). Listed B_s_{geod} is derived using Bw_{geod,ss}. Regional late summer snow density (Table 5) was used to calculate Ba_{geod}.

725

Year	Glacier	$Bw_{\text{geod,gl}} \pm \sigma_{\text{geod,bw}}$	$Bw_{\text{geod,sc}} \pm \sigma_{\text{geod,bw}}$	$Bs_{\text{geod}} \pm \sigma_{\text{geod,bs}}$	$Ba_{\text{geod}} \pm \sigma_{\text{geod,ba}}$	$Bw_{\text{glac}} \pm \sigma_{\text{glac,bw}}$	$Bs_{\text{glac}} \pm \sigma_{\text{glac,bs}}$	$Ba_{\text{glac}} \pm \sigma_{\text{glac,ba}}$	$Bw_{\text{surv,corr}}$	$Ba_{\text{surv,corr}}$	AAR	ELA (m)	NMAD Ba (m)	NMAD Bw (m)	Median Ba _{Δh} (m)	Bias _{Δh} (m)	$\bar{\rho}$ (kg m ⁻³)
2018	Zillmer	1.70 ± 0.19	1.75 ± 0.20			1.65 ± 0.17			-0.15							1.4	
2018	Nordic	1.87 ± 0.26	2.07 ± 0.27			2.18 ± 0.14			-0.04							1.76	
2018	Illecillewaet	1.61 ± 0.17	1.65 ± 0.18			—			na							2.26	
2018	Haig	1.25 ± 0.15	1.31 ± 0.19			1.42 ± 0.15			na							1.83	
2018	Conrad	1.62 ± 0.21	1.84 ± 0.23			1.83 ± 0.12			0.00							2.34	
2018	Kokanee	2.07 ± 0.25	2.31 ± 0.26			2.25 ± 0.13			0.01							1.76	
2017	Zillmer	2.12 ± 0.24	2.03 ± 0.25	-2.70 ± 0.27	-0.67 ± 0.10	1.93 ± 0.26	-2.44 ± 0.35	-0.51 ± 0.23	0.15	-0.31	0.48	2440	0.6	1.83	-0.1	-0.05	729 ± 45
2017	Nordic	2.14 ± 0.29	2.18 ± 0.30	-2.77 ± 0.31	-0.59 ± 0.09	2.03 ± 0.22	-2.78 ± 0.32	-0.75 ± 0.23	-0.04	-0.10	0.39	2540	0.28	1.8	0.01	-0.09	732 ± 43
2017	Illecillewaet	1.47 ± 0.19	1.54 ± 0.20	-2.55 ± 0.27	-1.01 ± 0.18	2.00 ± 0.16	-2.84 ± 0.32	-0.84 ± 0.28	—	—	0.36	2615	0.32	2.19	0.01	0	718 ± 49
2017	Haig	1.58 ± 0.20	1.65 ± 0.23	-3.56 ± 0.31	-1.91 ± 0.21	1.50 ± 0.17	-3.43 ± 0.29	-1.93 ± 0.24	—	—	0.04	na	0.31	1.62	0.01	0.04	885 ± 10
2017	Conrad	2.10 ± 0.22	1.91 ± 0.23	-2.97 ± 0.26	-1.06 ± 0.13	2.17 ± 0.17	-3.12 ± 0.29	-0.95 ± 0.24	-0.16	-0.16	0.48	2600	0.31	2.68	0	-0.01	730 ± 45
2017	Kokanee	3.15 ± 0.32	2.86 ± 0.33	-3.14 ± 0.34	-0.28 ± 0.08	2.84 ± 0.25	-2.87 ± 0.34	-0.03 ± 0.23	0.00	0.01	0.62	2560	0.34	1.99	-0.08	-0.01	711 ± 55
2016	Zillmer	1.68 ± 0.19	1.72 ± 0.20	-2.27 ± 0.22	-0.55 ± 0.07	1.99 ± 0.23	-2.61 ± 0.33	-0.62 ± 0.24	0.02	-0.38	0.49	2410	0.21	1.76	0.01	-0.02	726 ± 46
2016	Nordic	1.79 ± 0.22	1.70 ± 0.23	-1.85 ± 0.24	-0.15 ± 0.08	1.79 ± 0.14	-1.90 ± 0.21	-0.11 ± 0.16	-0.08	0.01	0.43	2555	0.16	1.63	0	-0.04	727 ± 40
2016	Illecillewaet	1.41 ± 0.17	1.46 ± 0.18	-1.73 ± 0.18	-0.27 ± 0.05	—	—	-0.19 ± 0.28	—	—	0.60	2550	0.45	1.9	-0.01	0.05	718 ± 54
2016	Haig	1.15 ± 0.15	1.21 ± 0.17	-2.27 ± 0.20	-1.06 ± 0.11	1.34 ± 0.17	-2.49 ± 0.29	-1.15 ± 0.24	—	—	0.03	na	0.38	1.24	-0.01	-0.04	893 ± 10
2016	Conrad	1.40 ± 0.18	1.47 ± 0.19	-1.74 ± 0.20	-0.27 ± 0.06	1.88 ± 0.12	-2.08 ± 0.20	-0.20 ± 0.16	0.11	-0.13	0.55	2530	0.14	2.1	0	-0.02	734 ± 50
2016	Kokanee	1.98 ± 0.22	2.05 ± 0.23	-1.93 ± 0.23	$+0.12 \pm 0.05$	2.07 ± 0.13	-1.94 ± 0.26	$+0.13 \pm 0.22$	-0.05	0.12	0.72	2545	0.15	1.67	0	0	681 ± 64
2015	Zillmer	—	—	—	—	2.06 ± 0.30	-2.82 ± 0.40	-0.76 ± 0.27	0.00	-0.32	0.30	2500	—	—	—	—	—
2015	Nordic	1.74 ± 0.22	1.81 ± 0.23	-2.81 ± 0.28	-1.0 ± 0.16	1.83 ± 0.19	-3.02 ± 0.31	-1.19 ± 0.24	-0.16	0.06	0.32	2610	0.26	1.76	0	0.02	744 ± 42
2015	Illecillewaet	—	—	—	—	—	—	-1.17 ± 0.47	—	—	0.30	2600	—	—	—	—	
2015	Haig	—	—	—	—	1.23 ± 0.25	-3.02 ± 0.25	-1.79 ± 0.25	—	—	0.00	na	—	—	—	—	
2015	Conrad	1.65 ± 0.17	1.64 ± 0.18	-3.06 ± 0.24	-1.42 ± 0.16	1.80 ± 0.13	-3.20 ± 0.35	-1.40 ± 0.32	-0.02	-0.31	0.44	2685	0.21	2.2	-0.01	-0.03	736 ± 43
2015	Kokanee	—	—	—	—	2.18 ± 0.29	-3.38 ± 0.40	-1.20 ± 0.28	0.00	—	0.20	2680	—	—	—	—	
All	Average	1.87 ± 0.11	1.88 ± 0.09	-2.59 ± 0.16	-0.76 ± 0.16	1.95 ± 0.08	-2.67 ± 0.13	-0.73 ± 0.15	-0.04	-0.14	0.38	2553	0.29	1.89	-0.01	-0.01	748 ± 62

Table 4: Density values used for geodetic and glaciological balance. Glaciological values are average values.

Density	Geodetic (kg m ⁻³)	Glaciological (kg m ⁻³)	n
ρ_{spring}	$470 \pm 70^*$	$457 \pm 50^*$	74
ρ_{snow}	590 ± 90	570 ± 20	27
ρ_{firn}	700 ± 100	703 ± 65	4
ρ_{ice}	910 ± 10	—	—

*Geodetic spring snow density (ρ_{spring}) is $440 \pm 50 \text{ kg m}^{-3}$ for Haig Glacier and glaciological is $420 \pm 45 \text{ kg m}^{-3}$ (n = 46).

Table 5: Late summer snow density observations from regional studies. We use 570 kg m⁻³ as our density of late summer snow for geodetic mass balance, but also separately calculate mass balance using the average for regional studies excluding those from glaciers in this study (590 kg m⁻³).

Location	Mean	Range	References
	ρ_{snow} (kg m ⁻³)	ρ_{snow} (kg m ⁻³)	
South Cascade Gl., WA, USA	580	530 – 600	(Bidlake et al., 2010; Krimmel, 1996)
Juneau Icefield, AK, USA	560	540 – 580	(Miller and Pelto, 1999; Pelto and Miller, 1990)
Castle Creek Gl., BC, CA	600	—	(Beedle et al., 2014)
North Cascades, WA, USA	600	590 – 630	(Pelto and Riedel, 2001)
Haig Glacier, AB, CA	545	530 – 570	(Marshall, 2012)
Columbia Basin, BC, CA	570	535 – 615	This study

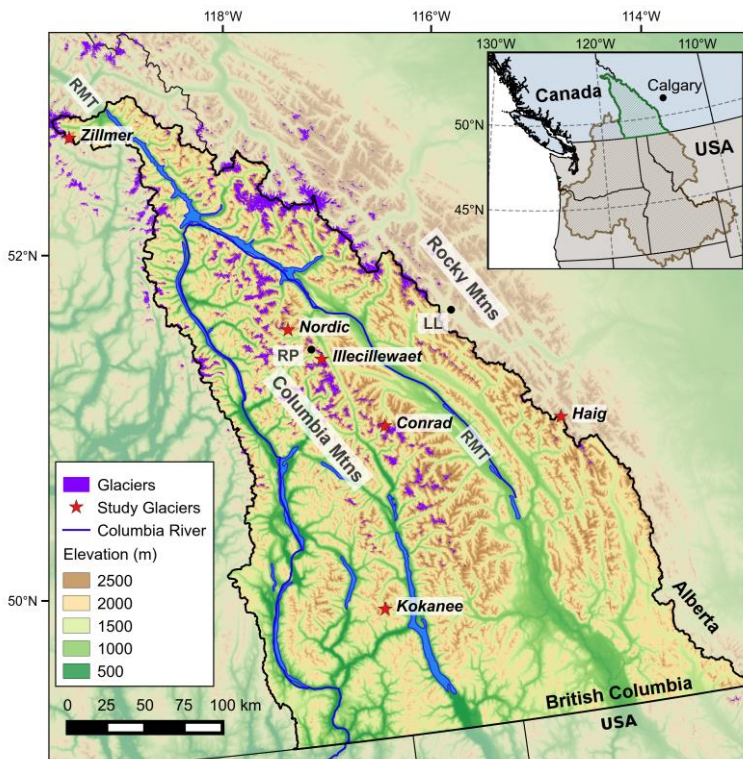


Figure 1: Map of the Canadian Columbia River Basin (black outline, brighter topography) and locations of study sites. Inset shows regional context of the Canadian portion of the Columbia River Basin which contributes to the river when it crosses the international border (green). The remainder of the basin is also depicted (brown). The Columbia and Rocky Mountains are separated by the Rocky Mountain Trench (RMT). Weather stations (black dots) at Rodgers Pass (RP) and Lake Louise (LL) are referred to in the introduction. Map coordinates are in NAD83/BCAlbers.

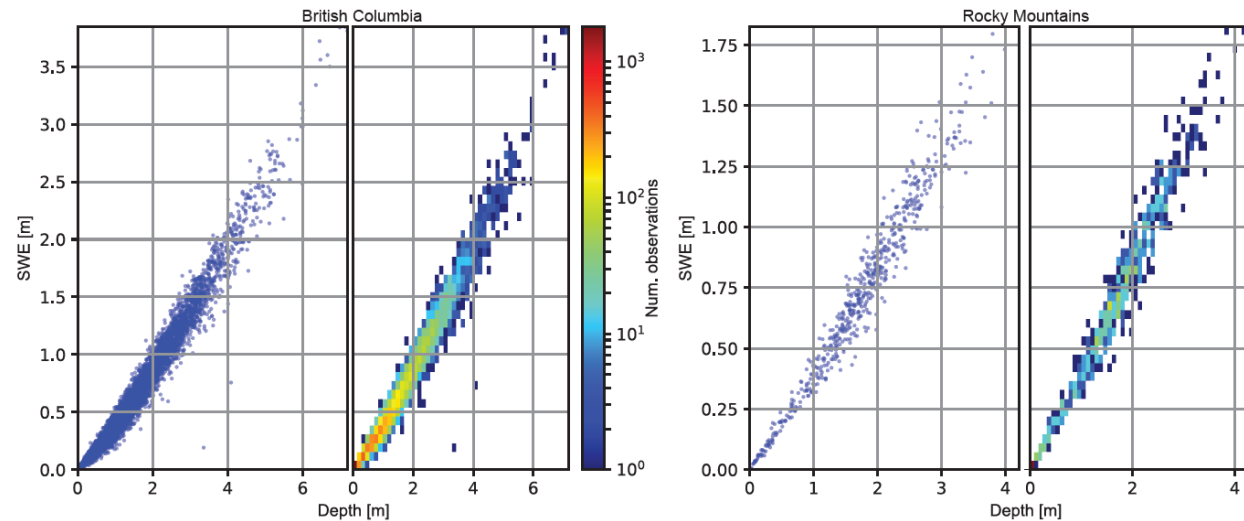
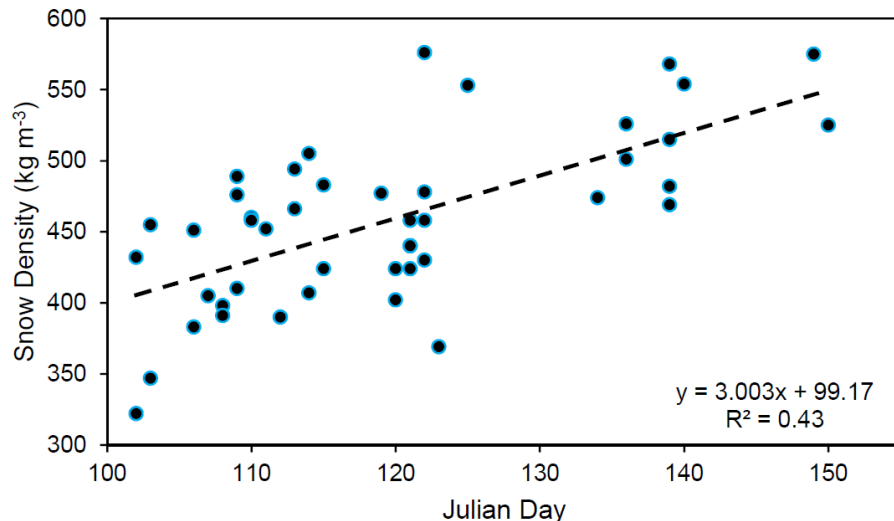


Figure 2: Snow depth versus snow water equivalent from May 1 provincial snow survey data. The mean date of our spring field seasons was May 1, and so we chose May 1 BC snow survey data (left) to derive a SWE/snow depth regression from which we

determined the average May 1 snow density ($470 \pm 70 \text{ kg m}^{-3}$ ($r^2 = 0.97$, $n = 10,169$)). For Haig Glacier, we derived a regression from only snow stations within the Rocky Mountains south of Pine Pass to derive winter density ($440 \pm 50 \text{ kg m}^{-3}$ ($r^2 = 0.97$, $n = 629$)).



755

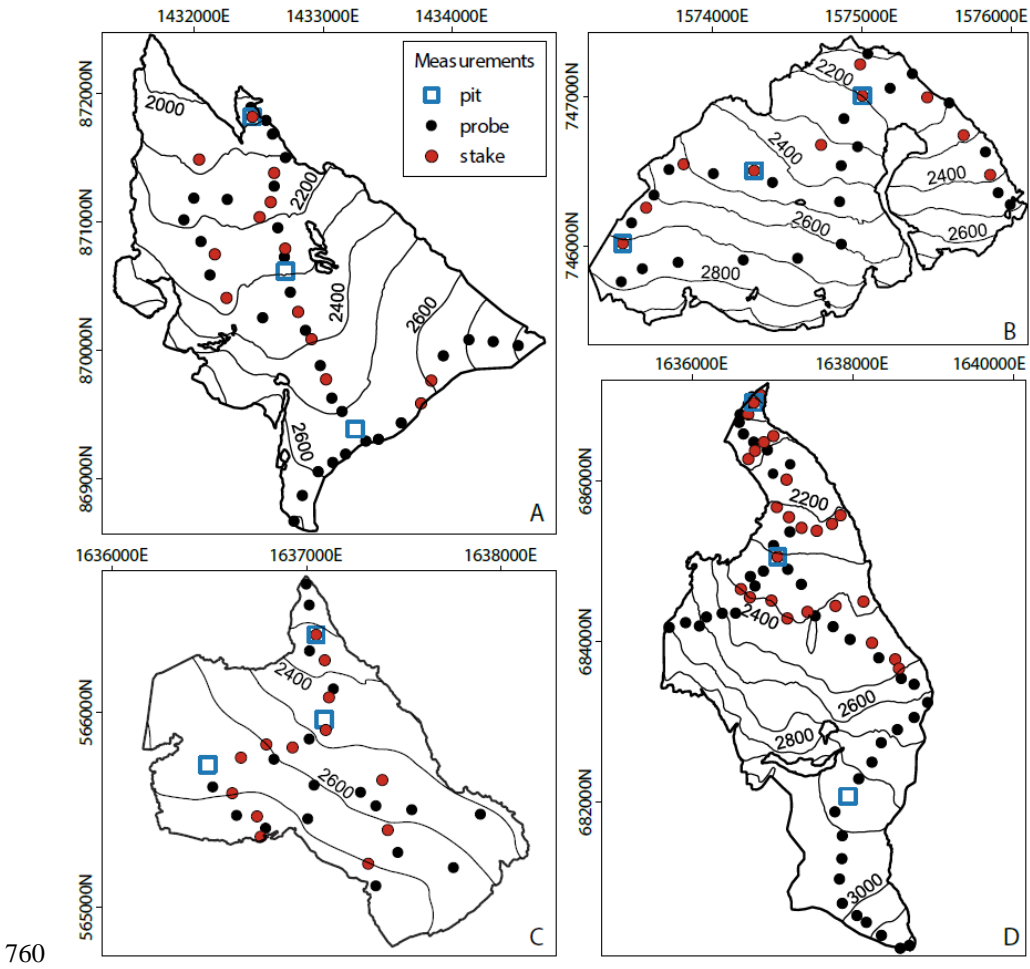
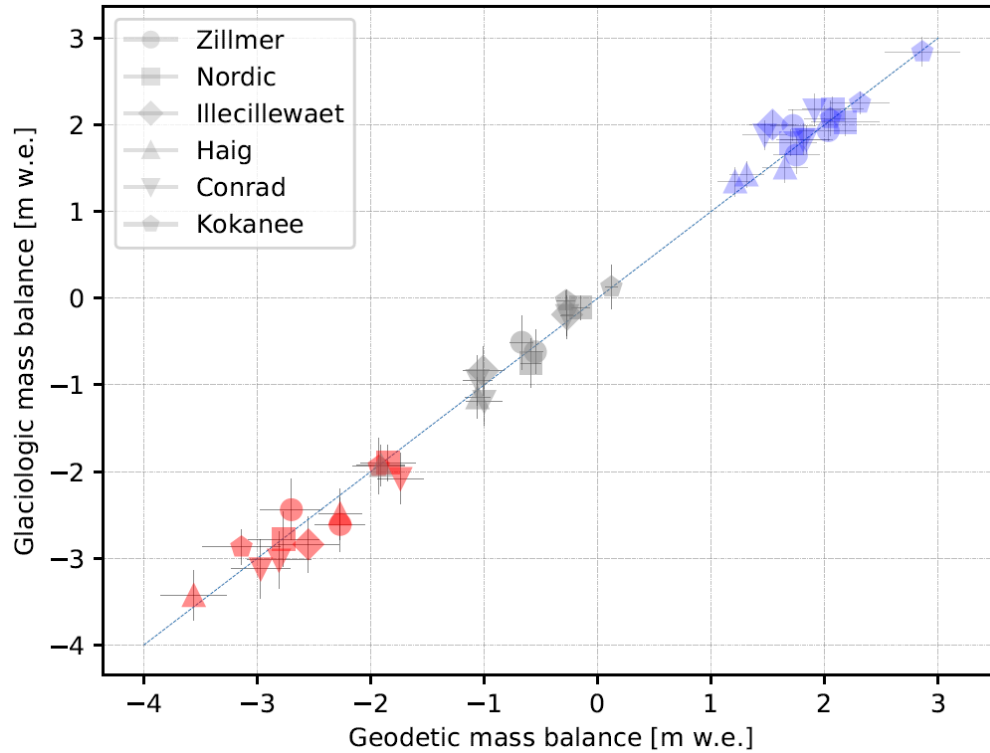


Figure 4: Measurement networks for the A) Zillmer, B) Nordic, C) Conrad, and D) Kokanee glaciers. Snow depth measurement locations, ablation stakes, and snow pit/core locations are pictured. Refer to Marshall et al. (2014) for the Haig Glacier, and Hirose and Marshall (2013) for the Illecillewaet Glacier. Map coordinates are in WGS84/UTM11N.

765



770 **Figure 5: Geodetic versus glaciological mass balance estimates for 2015 through 2018 for all six study glaciers with a one-to-one line.** Winter balance (blue) covers the accumulation season from mid-September to late April, summer balance (red) spanning the remaining months, and annual balance (grey). Errors depicted are 1σ uncertainties. Average $B_{w\text{-glac}}$ was 4% greater than $B_{w\text{-geod}}$, and $B_{s\text{-glac}}$ and $B_{a\text{-glac}}$ were 4% greater than our geodetic estimates on average.

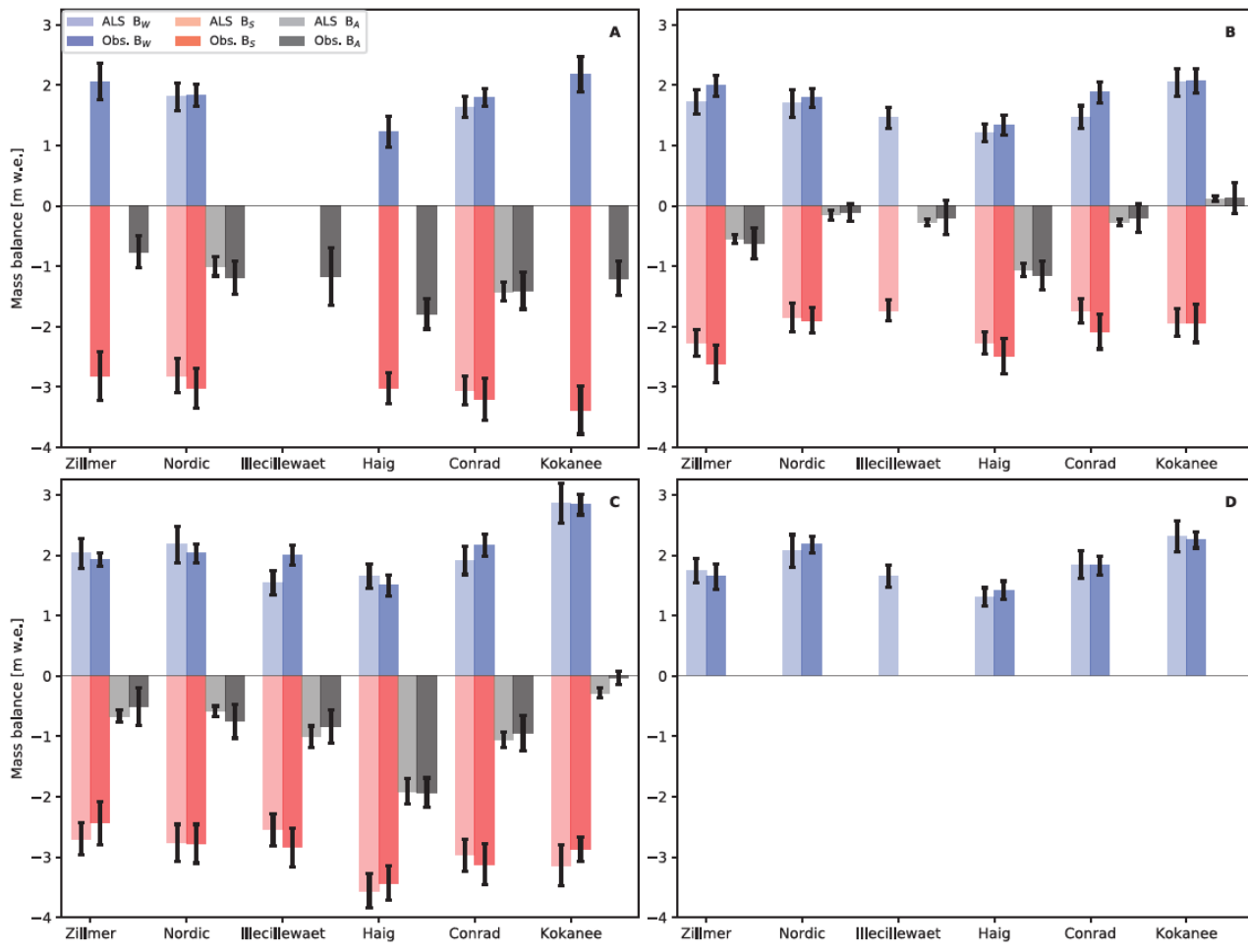


Figure 6: Seasonal and annual mass balance for all study glaciers from both geodetic and glaciological measurements for each balance year from 2014 to 2018 with 1σ uncertainties. A) 2014 to 2015 balance year, B) 2015 to 2016 balance year, C) 2016 to 2017 balance year, D) 2017 to 2018 winter balance.

780

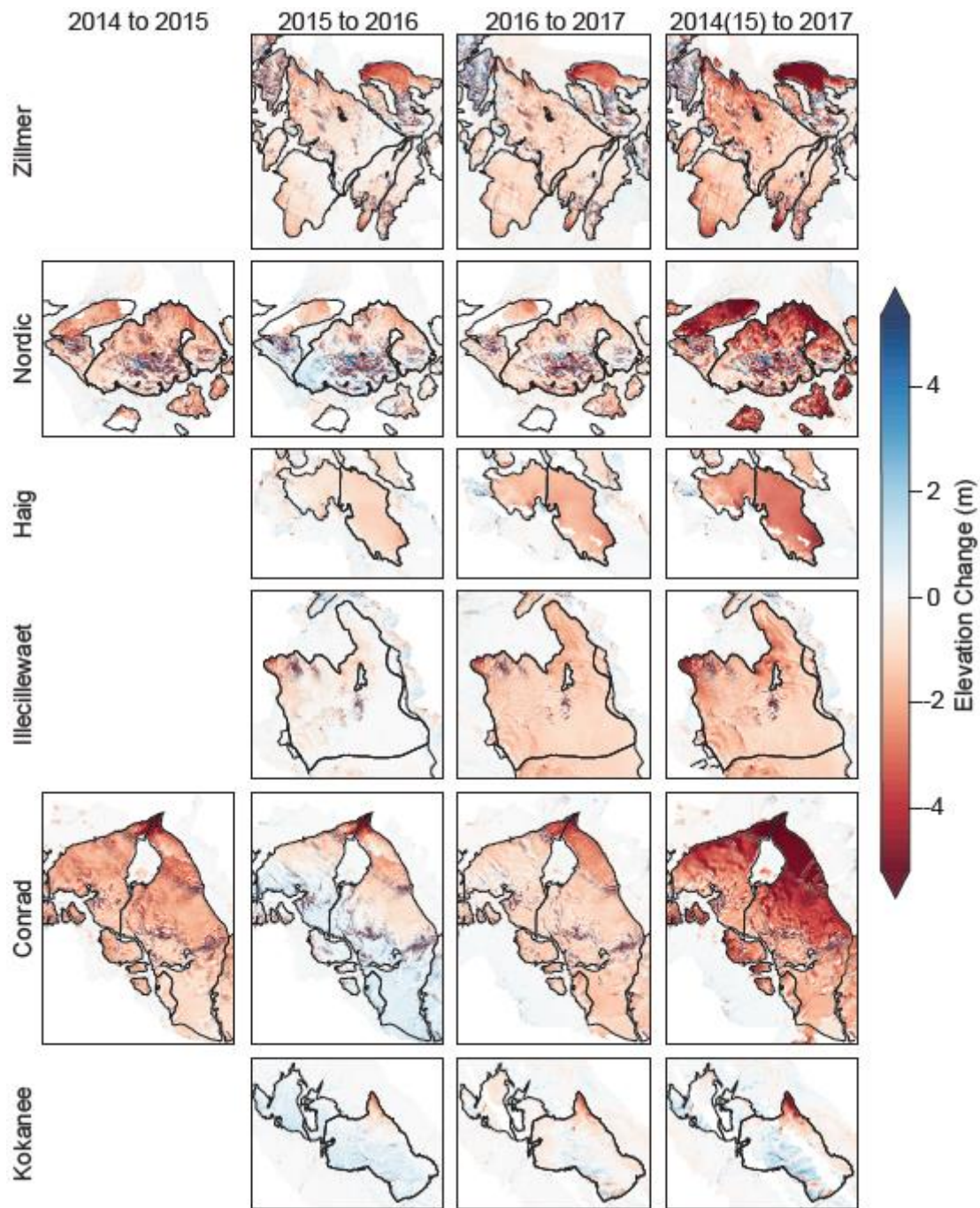


Figure 7: Surface height change for the Zillmer, Nordic, Haig, Illecillewaet, Conrad, and Kokanee glaciers from the first late summer DEM (2014 or 2015) until late summer 2017. Study glaciers are outlined with thick black line and other glaciers with a thin black line. Off-ice areas deemed stable terrain were used for error analysis and coregistration.

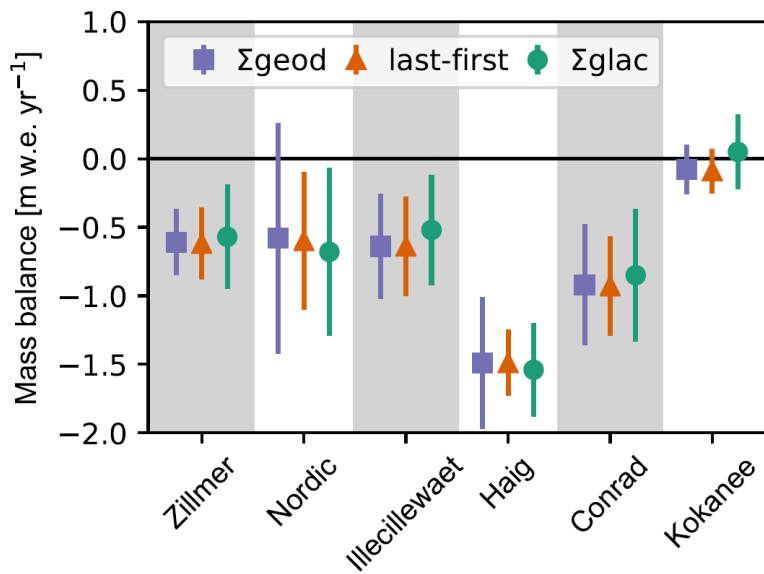


Figure 8: Summed annual mass balance from glaciological data (Σ_{glac}), geodetic data (Σ_{geod}), and last-first ΔDEM . Last-first ΔDEMs were created by differencing the first available DEM (2014 or 2015 late summer) from the last available DEM (2017) for each site (Table 2). Errors denote 2-sigma uncertainties.

790

795